

**MICRO PUMPING AND PARTICLE SEPARATION/COLLECTION
USING OSCILLATING BUBBLES**

by

Kyungjoo Ryu

B.S., Sungkyunkwan University, South Korea, 2002

Submitted to the Graduate Faculty of
Swanson School of Engineering in partial fulfillment
of the requirements for the degree of
Master of Science

University of Pittsburgh

2008

UNIVERSITY OF PITTSBURGH
SWANSON SCHOOL OF ENGINEERING

This thesis was presented

by

Kyungjoo Ryu

It was defended on

July 10, 2008

and approved by

Dr. Jeffrey Vipperman, Associate Professor,
Department of Mechanical Engineering and Materials Science

Dr. Laura Schaefer, Associate Professor,
Department of Mechanical Engineering and Materials Science

Thesis Advisor: Dr. Sung Kwon Cho, Assistant Professor,
Department of Mechanical Engineering and Materials Science

Copyright © by Kyungjoo Ryu

2008

MICRO PUMPING AND SEPARATING/COLLECTING PARTICLES USING OSCILLATING BUBBLES

Kyungjoo Ryu, M.S.

University of Pittsburgh, 2008

When a gaseous bubble in liquid is excited by acoustic waves, it oscillates in harmony with the wave and generates strong vortical flows around it, so-called cavitational microstreaming. In this thesis, the microstreaming phenomenon is investigated in development of two microfluidic devices: micropump and microparticle separator. In the micropump, the key idea is to vertically place a capillary tube above the oscillating bubble to collect the upward microstreaming flow into the tube. When the bubble is excited at its resonance frequency, it oscillates with surface undulations (surface wave mode) and pumps water through the tube. The performance of micro pumping is experimentally studied in various conditions in terms of the generated flow rate and pressure. The maximum flow rate and generated pressure are measured at $\sim 0.7 \mu\text{l}$ and 1.8 Pa , indicating that the present pump falls into high-flow-rate and low-pressure type pumps. The present pump runs without physical connections or electric wiring to bubbles, implicating potential applications of implantable micropumps.

The microparticle separator utilizes the recently-discovered phenomenon that the oscillating bubble attracts and captures large neighboring objects, not small objects ($< 20 \mu\text{m}$). This capturing principle is evaluated in three different microfluidic configurations: mini- and micro-channels and microchamber. Single or multiple microbubbles are deposited on Teflon-patterned spots or microcavities in the channel and oscillated by an acoustic wave. When a mixture solution with 80- and $2\text{-}\mu\text{m}$ particles is injected into the channels, only the $80\text{-}\mu\text{m}$

particles are captured near the oscillating bubbles while the 2- μm particles pass the bubbles without being captured. By simply turning off the acoustic wave, the captured 80- μm particles are easily released. A similar capturing (separating) operation is achieved in the microchamber. Since the filled water in the microchamber is quiescent, oscillating bubbles need to move in the chamber to selectively capture 80- μm particles suspended in the chamber. 2-D movements of oscillating bubbles are achieved by sequentially activating arrayed square electrodes on the chamber bottom surface, so-called electrowetting-on-dielectric (EWOD). When the bubble is simultaneously actuated by EWOD and acoustic excitation, it captures and carries 80- μm particles, not 2- μm particles.

TABLE OF CONTENTS

1.0 INTRODUCTION	1
2.0 MICRO PUMPING USING AN OSCILLATING BUBBLE	5
2.1 BACKGROUND	5
2.2 EXPERIMENTAL SETUP	8
2.3 RESULTS AND DISCUSSION	12
2.3.1 Initial condition and bubble shape	12
2.3.2 Zero flow rate state	14
2.3.3 Pumping by oscillating bubble	16
2.3.4 Dependence of flow rate on the back pressure	19
2.4 SUMMARY	24
2.5 FUTURE WORK	26
3.0 SEPARATION AND COLLECTION OF MICROPARTICLES USING OSCILLATING BUBBLES	27
3.1 BACKGROUND	27
3.2 EXPERIMENTAL SETUP	29
3.2.1 Particle separation and collection in a minichannel	30
3.2.2 Particle separation and collection in a microchannel with cavities	35
3.2.3 Particle separation and collection in a microchamber using mobile oscillating bubble	39
3.3 SUMMARY	43
3.4 FUTURE WORK	44
4.0 CONCLUSION	46
BIBLIOGRAPHY	48

LIST OF TABLES

Table 1 Additional pressure load due to the contact angle difference	24
--	----

LIST OF FIGURES

Figure 1 Streamlines of acoustic streaming.....	7
Figure 2 Illustration of experimental setup.....	11
Figure 3 Initial condition of bubble under various acoustic wave.....	12
Figure 4 The bubble with the tube installed is excited at four different actuation frequencies....	13
Figure 5 Pressure generation by the oscillating bubble	14
Figure 6 Flow generation by bubble pump.....	16
Figure 7 The effect of the inner diameter of the tube on velocity and flow rate.	17
Figure 8 The effect of the vertical position of the tube inlet (δ / r) on the velocity.....	18
Figure 9 Pressure drop in the tube.	18
Figure 10 Micropump configuration.....	19
Figure 11 Dependence of the flow rate on the water level difference between the left and right reservoirs.....	21
Figure 12 Total pressure load vs. flow rate.....	22
Figure 13 Difference of the contact angles.	23
Figure 14 Sequential pictures showing that acoustically excited oscillating bubbles can separate particles of two different sizes.	28
Figure 15 Experimental setup for particle separation and collection with fluidic devices.....	29
Figure 16 Perspective view of minichannel configuration for particle separation and collection.	31
Figure 17 Microfabrication steps of minichannel.	32
Figure 18 Single bubble case in minichannel	33
Figure 19 Two bubbles (250 μm dia.) of the same size are excited at 24 kHz.....	34
Figure 20 Configuration of collection and separation in a microchannel with cavity.....	35
Figure 21 Fabrication steps of particle separating/capturing in a channel with cavities	36

Figure 22 Sequential images of automatic bubble deposition on cavities in the microchannel. ..	37
Figure 23 Sequential images of particle capturing and separating in the microchannel with cavities.	38
Figure 24 Configuration of collection and separation in a microchamber by a mobile oscillating bubble.....	39
Figure 25 Microfabrication steps of microchamber testing device	40
Figure 26 Schematic of activation signal flow for EWOD bubble operation.....	41
Figure 27 A bubble of 250- μm diameter is transported to the left by EWOD and oscillated by acoustic excitation.....	42

1.0 INTRODUCTION

Bubbles exist everywhere, typically in a globule shape which is a lower energy state (for example, water vapor in boiling water, nucleation of carbon dioxide in soda, actuator in a inkjet printer, and so on). As such, bubbles have been around for a long time as popular research topics in the areas of physics, chemistry, engineering, and medicine [1, 2]. In particular, since microfluidics emerged, tremendous attentions have been drawn to bubbles. In microfluidics applications, bubbles are viewed in two opposite ways: something to be avoided and something to be utilized. Contractions, expansions, and geometrical changes in narrow microchannel passage are prone to cause clogging problems associated with bubbles [3-5]. On contrary, bubbles are often utilized as an actuation source to generate strong forces since interfacial tension of bubbles dominates other types of forces in microscales. So far, a variety of methods for bubble control and application have been reported.

The most successfully commercialized application of bubbles would be ink jet printers. Rapidly growing bubbles via local heating squeeze ink in the chamber and push ink droplets out of the nozzle [6]. In research stages, many bubble actuators have been developed as well. In Lin [7], bubbles thermopneumatically reciprocated membranes to displace and pump fluid in the chamber. In the following work, Lin et al [8] directly used bubbles to generate reciprocating motions in fluid without membranes. In particular, their pump was integrated with the nozzle and diffuser at the inlet and outlet. This configuration can generate a net flow in one direction

without valves, as the operational mechanism was first introduced by Olsson [9]. Generating bubbles in the confined microchannel can pump the fluid through the channel as demonstrated by Yuan and Prosperetti [10]. In their pump, a bubble was generated on a platinum heater on the top of a quartz substrate. Jun and Kim [11] demonstrated that sequential heating of the bubble in the microchannel can move the bubble through the channel, resulting in pushing the filler liquid in the channel. This bubble driving mechanism is related to asymmetric vapor pressure and surface tension in the bubble due to the temperature gradient along the channel. In the meantime, thermally grown bubbles can be used for capturing micro bio objects. In reference[12], a thermally growing and shrinking bubble transmits pressure through a conduit, of which end tip thus captures and releases objects with no direct contact between the bubble and objects. This non-contact manipulation could minimize thermal and mechanical damage on the objects [13]. In the above applications, the bubbles are generated and actuated by thermal heating, which means that this mechanism requires significant power for successive operations. The power requirement becomes more problematic as the device scale goes down since heat dissipation becomes more prominent.

The other approach to generate and actuate microbubbles is the electrochemical method, so called electrolysis. A wide variety of applications using electrochemically generated bubbles have been studied and developed such as pumps, dispensing systems, optical switches, and so on [14-17]. The main advantage of electrochemical bubble generation is that the bubble temperature is close to room temperature. However, bubbles can be generated only in electrolyte solutions.

Another method for actuating bubbles is acoustic (or ultrasound) excitation. Since gaseous bubbles in liquid media are compressible, in the presence of pressure waves (acoustic wave) they oscillate in harmony with the frequency of the wave. It is known that bubble

oscillation generates strong vortical non-zero flows around the bubble, so called cavitation microstreaming flow [18]. Depending on the frequency and amplitude of the excitation wave, the bubble undergoes different modes in oscillating motions: translational, axisymmetric, and surface wave modes (Elder [19] and Tho [20]). The translating oscillation is that the bubble oscillates along one or more lateral axes. Typically, this mode occurs at the excitation frequencies much lower than the bubble resonance frequency. As the excitation frequency increases, the mode is transitioned to the axisymmetric mode. The bubble is repeatedly expanded and shrunk with keeping its spherical shape. In other word, this is volume oscillation. When the excitation frequency is close to the bubble resonance frequency, the mode becomes surface wave mode. The bubble deforms into polygonal shape. The surface wave mode is more complex and not clearly understood yet as compared to the translational and axisymmetric modes. However, the microstreaming velocity of the shape mode is measured 2~3 times larger than those in the translating and axisymmetric modes.

Recently, oscillating bubbles and cavitation microstreaming have spawned many potential applications. As a commercial and clinical application, bubbles are frequently used as ultrasonic-imaging contrast agents to highlight the specific parts of the body [21-23]. In addition, these agents have potential implications for delivering drugs or molecules to some parts of the brain without disturbing others [24]. In this case, the drug and molecules can be bound to the bubble surface and released upon external ultrasound excitation. In addition, it is shown Marmottant and Hilgenfeldt [25] that the cavitation microstreaming flow generated by the oscillating bubble enhance the permeability of the adjacent cell membrane. As a result, the drug and molecules can be delivered into the target cells by the ultrasound excitation. The cavitation flow can be steered by the surrounding solid objects as Marmottant and Hilgenfeldt [26]. If well

controlled, this mechanism may be used to control micro flows in the channel. In addition, some attempts such as vortex generator and micro particle carrier [27-29] have been made to utilize the cavitation microstreaming flow. As briefly reviewed above, oscillating bubbles offer new functionalities and many advantages in their operations, as compared to the thermal and electrochemical methods. However, their studies and applications still remain in the primitive level as of today.

In this thesis, the cavitation microstreaming flow is investigated in the development of two novel microfluidic devices: micropump and microparticle separator. Although the two devices have different functionalities, they are commonly actuated and driven by oscillating bubbles. To generate the microstreaming flow, bubbles are excited near at the resonance frequencies using a bulk piezo actuator, and thus oscillation mode is identified as surface wave mode. In the following chapters, their working principles, device fabrications, and testing results will be presented.

2.0 MICRO PUMPING USING AN OSCILLATING BUBBLE

2.1 BACKGROUND

Development of MEMS (Microelectromechanical Systems) has had a great impact in microfluidics, miniaturizing macroscale fluid operations and thus realizing various handheld systems for biomedical, homeland security applications. In these systems, commonly required fluid operations are pumping [30, 31], mixing [32-34], valving [35], separating [36, 37], collecting [38, 39], etc. Among these, micropumping is most critical and important as over 200 journal papers on micropumping have been published since Smits' micropump in year 1990 was developed for the first time [40]. In the beginning of microfluidics era, the main focus of micropump research was placed on reciprocating displacement type micropumps with moving actuators. Analogy with moving boundaries such as pistons in macroscale pumps, deformable microscale plates or membranes are miniaturized for the moving boundary components to generate high pressure. As a result, the pumping principle is based on pressure-driven flows. Depending on the actuation principle of microplates or membranes, this reciprocating displacement type micropumps could be sub-categorized: piezoelectric disk actuator[9, 40], electrostatic force[41, 42], thermopneumatic force[43, 44], shape memory alloy[45], electromagnetic[46], electrowetting[47], and so on.

The concept of piezoelectric disk actuator is that when the voltage is applied to piezo material, the material deforms and thus displaces the contact fluid [9, 40]. Piezoelectric micro pump can be actuated at relatively high frequency. Micropumps using electrostatic force are performed by electrostatically actuated membranes [41, 42]. The force generates a membrane downward deformation, which is then recovered by removing the electric potential. The structure of the pump is complex, and the high voltage is typically required. The thermopneumatic force is also used for micropumping [43, 44]. Air inside the pump is expanded and compressed by the heater and cooler. This continuous motion displaces the fluid. However, the response time is relatively slow and the required power is pretty high. The shape memory alloy is frequently used for generating reciprocating motions for micropumping [45]. Pumping process is made by restoring its original shape after heating/cooling cycles. The material should be sustained under high stress and long cycles even though it needs high power consumption. The electromagnetic micropump [46] consists of a permanent magnet placed in a coil and a flexible pump membrane.

As the scale goes down to micro scale, the above pressure-driven methods are not efficient driving sources for pumping since the required pressure drop is proportional to the fourth power of flow passage diameter. As alternatives to the pressure, attentions have been drawn to harnessing other dominant forces in the microscale that were typically considered negligible in many macro scale applications. Such dominant forces includes surface tension (thermocapillary and electrocapillary [48, 49]), electrohydrodynamic[50, 51], electroosmotic[52, 53], magnetohydrodynamic[54, 55] and acoustic [56]. In the past decades, understanding and development of these pumping principles have been significantly advanced. Currently, some of them are proven efficient even in practical-level applications. Among many, the most important advantages of these pumping principles are that they do not necessarily require moving parts,

thus resulting in simple fabrication. In general, however, the applicability of the principles is limited to particular fluids and conditions, as opposed to the pressure that can be used for virtually all kinds of fluids.

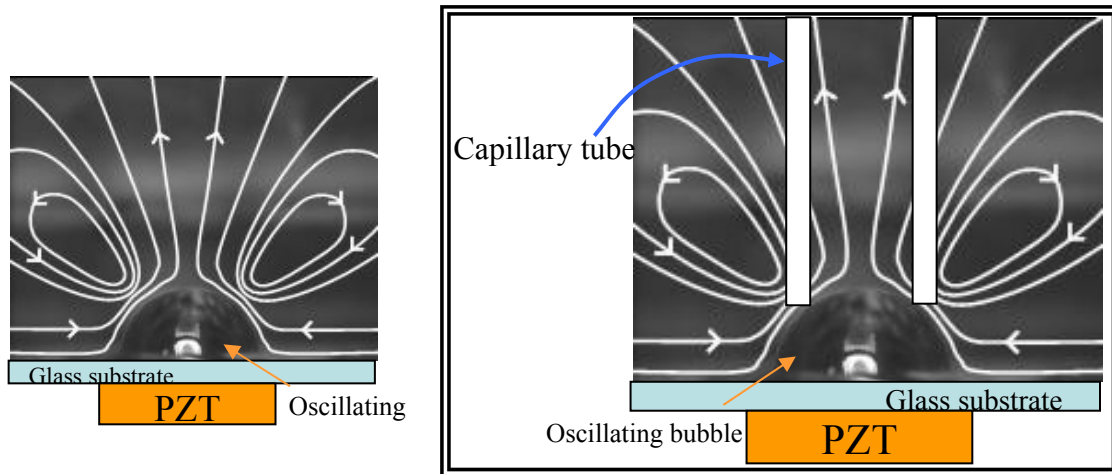


Figure 1 Streamlines of acoustic streaming. The bubble is acoustically excited at its resonance frequency. As a result vortical flows are generated around the bubble. The key concept of the present pumping principle is to collect only upward flows in the acoustic streaming into a capillary tube.

As the first topic of this thesis, this chapter describes a new micropumping principle using acoustically-excited oscillating microbubbles. This pump harnesses the cavitation microstreaming flow generated by the oscillating bubble (Figure 1). When the frequency is close to the bubble resonance frequency and thus the bubble oscillation amplitude is large enough, the general flow patterns are similar to the toroidal vortical structure as shown in Fig. 1; nearly straight flows near the bubble center and circulating flows in the sides of the bubble. The key idea in the present pumping principle is confining and collecting the straight flow near the bubble center into a flow passage such as capillary tube. To prove this idea, a capillary tube is

placed on the top of the oscillating bubble, and the flow rate and pressure drop in the capillary tube are measured. The present pumping principle implicates implantable micropumps to deliver and release drugs since it does not require any physical and electrical wiring to the pump. To activate pumping, acoustic waves can be wirelessly applied from an external acoustic transducer to the target spots. In the following sections, the detailed experimental setup and the testing results will be presented. Although the scale in the present testing is not in the microscale, the proof of experiment can be a ground work for the next level miniaturization and integration.

2.2 EXPERIMENTAL SETUP

Figure 2 shows the experimental setup where a capillary tube is situated on the top of the bubble. A plastic rectangular parallelepiped reservoir (PVC, 30 mm × 20 mm × 20 mm) is filled with DI water. For the acoustic actuation, a ring-shaped bulk piezo actuator (Omega Piezo Technologies Inc., 20 mm in diameter) are directly bonded using double-side tape to transmit the acoustic vibration to the water reservoir. A parylene coated glass plate (10 mm × 10 mm × 1 mm) is placed on the bottom of the reservoir. An air bubble is injected on the plate using a micropipette. Due to the hydrophobicity of the parylene layer on the plate, the bubble is resting with a contact angle of approximately 90° on the substrate without floating off the plate. Otherwise, the bubble (for example, on a hydrophilic glass plate) would have tendency to detach from the plate due to buoyancy. A sine wave with an offset is generated by a function generator (33220A, Agilent Technologies), then amplified by a power amplifier (PZD700, TRek), and finally applied to the piezo actuator. As a consequence, the piezo actuator generates an acoustic vibration, which passes the plastic chamber and the glass substrate and reaches the water medium. The frequency

of the sine wave is adjustable but in most of the experiments set at the resonance frequency of the bubble. When the bubble diameter a is between 1 and 2 mm, the excitation frequency ranges between 2 and 6 kHz. The resonant frequency of the bubble f_b can be roughly predicted based on the Minnaert equation [57] :

$$f_b = \frac{1}{2\pi R_0} \sqrt{\frac{3\gamma p_0}{\rho}}, \quad (1)$$

where ρ denotes the mass density of the surrounding liquid, γ is the specific heat ratio of the gas, p_0 is the steady state pressure, R_0 is the steady state radius. This equation was valid only for suspended spherical bubbles, which is derived by comparing the kinetic energy of the liquid with the maximum internal energy of the gas within the bubble. The assumptions are negligible heat flow and negligible surface tension. For air bubbles in water in the standard condition, the equation may be reduced to the form: $f_b \cdot R_0 \approx 3 \text{ m/s}$ [18]. However, this equation is developed for spherical bubbles not hanging bubbles in the present experiment. So the resonance frequency is experimentally determined more accurately at which the bubble oscillation amplitude becomes maximum while the excitation frequency is being swept near the predicted frequency with a 10 Hz increment. In this process, captured regular- or high-speed images are used.

To collect the upward straight flows near the bubble center, a capillary tube is placed and held vertically above the bubble center tube using an accurate 3D traversing system (Fig. 2). The system allows accurate control of the distance between the bubble and the tube inlet. In this configuration, the resonant frequency of the bubble is slightly lower than that without the capillary tube because the tube disturbs the overall cavitation flow streaming around bubble. In particular, in case that the tube is misaligned off the bubble center to some extent, it is found that the resonant frequency significantly changes from the resonance frequency without the tube and

thus the collected flow becomes weaker. In addition, the resonant frequency of the bubble also changes as the distance between the bubble and tube inlet changes.

To visualize the flow and measure the flow rate in the tube, micro particles (green fluorescent polymer microspheres, 1% solids, Duke scientific Corp.) are initially seeded in the water medium. Since the particle density (1.05 g/cm^3) is similar to the one of the water, the particles are suspended in water. The particle diameter is $10 \text{ }\mu\text{m}$; small enough to trace the flow without slip but large enough to provide clear and bright flow tracing images. In order not to disturb the flow or movement of the bubble, the particle population is controlled in the proper range of $500 \sim 1000$ per $100 \text{ }\mu\text{l}$. To measure the flow rate in the tube, the seeded particles are traced far downstream of the tube inlet where the flow becomes a fully developed laminar pipe flow. Assuming that the velocity profile across the tube cross section is parabolic, the flow rate is inferred after averaging the maximum velocity of the particles in the tube which is read from the captured particle images.

While the bubble is oscillating, its shape and oscillating mode are taken using a high-speed digital camera (Phantom v7.3). Pictures can be taken up to 100,000 frames per second, fast enough to have 25 frames in one period of 4 kHz actuation. Here, such a high frame rate raises a concern of limited exposure time in each frame so the picture taken is not clear enough. Therefore, the light intensity should be fully increased as the actuation frequency is increased. To facilitate to provide highly intensified light continually, a halogen lamp (OSRAM ENH, 250W) is used. One may concern that the lamp generates heat, thus increasing the temperature of operating fluid in the testing setup. However, due to the large amount of water in the chamber, the temperature increase is negligible.

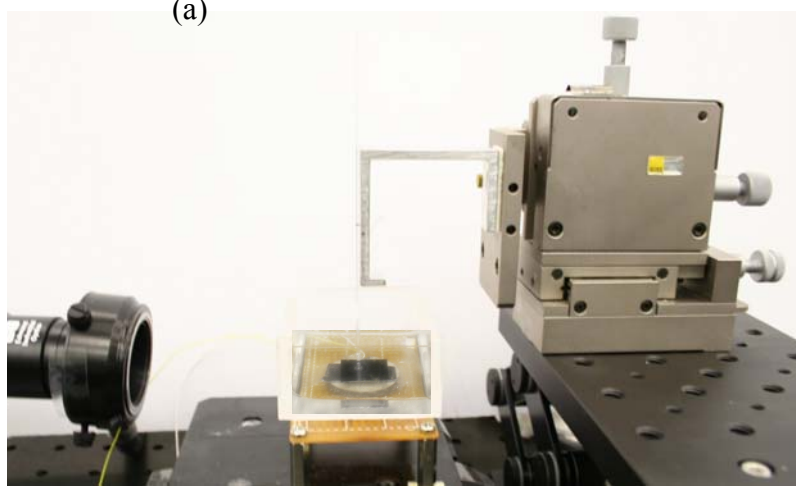
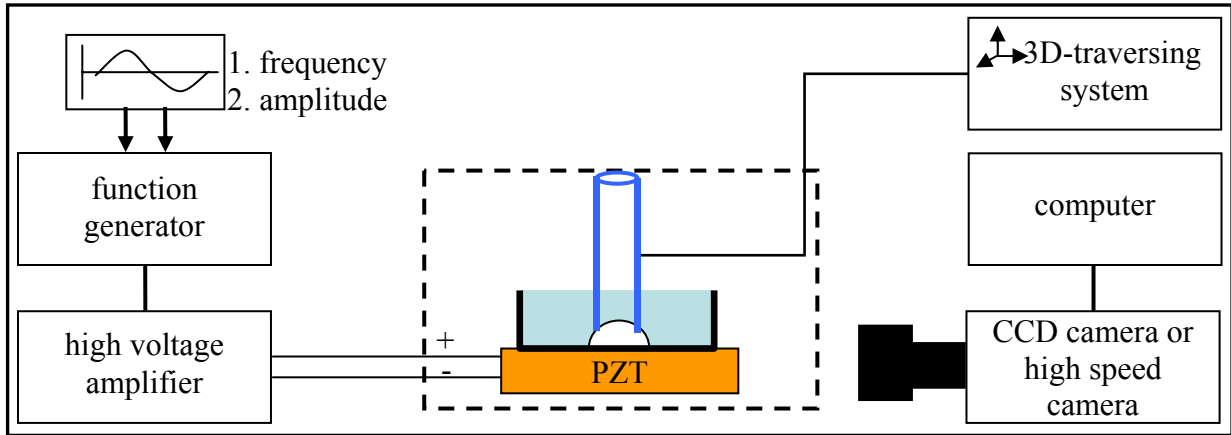


Figure 2 Illustration of experimental setup (a) experimental schematic diagram (b) function generator and power amplifier (c) high speed camera (d) microscope, testing device and 3-d traversing system.

2.3 RESULTS AND DISCUSSION

2.3.1 Initial condition and bubble shape

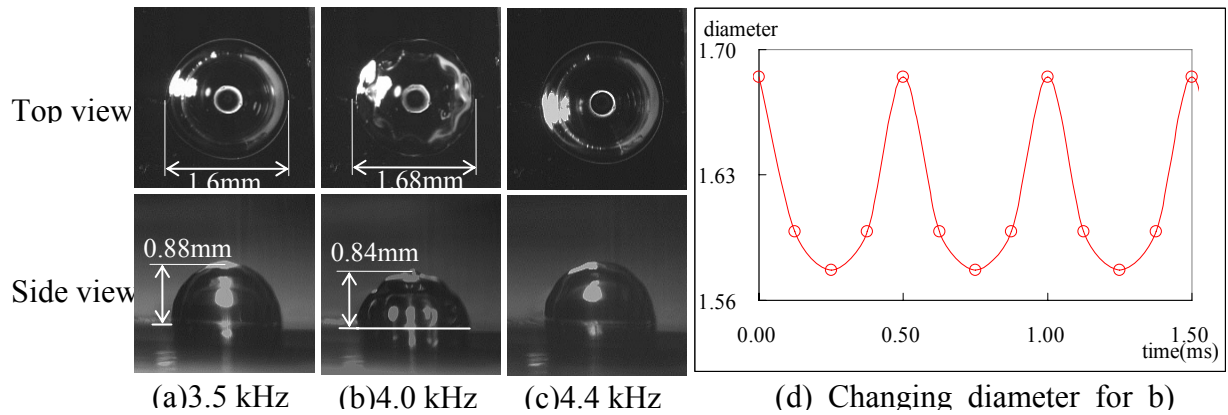


Figure 3 Initial condition of bubble under various acoustic wave (a)~(c)1.6mm bubble oscillation at 3.5, 4.0 and 4.4 kHz (d) changing diameter at the largest circumference for (b) case

Figures 3 (a), 3 (b), and 3 (c) illustrate that top views and side views of a 1.6mm oscillating bubble when excited at 3.5, 4.0, and 4.4 kHz, respectively, without the capillary tube installed. The pictures are taken at 32,700 frames per second using the high-speed digital camera (Phantom v7.3). At 4.0 kHz, which is the resonance frequency in this configuration [20, 58], the bubble oscillation is most prominent with surface undulations, so-called “surface wave mode”. In the top view the bubble has 11 undulation cycles along its circumference while 5 undulation cycles in the side view. Figure 3 (d) shows how the diameter changes in the time domain. The bubble diameter is measured at a slightly higher position than the contact line where the first anti-node in undulation is noticeable. The contact line of the bubble is considered as the node. This

measurement position is consistently taken when the tube is installed. In Figure 3 (d), the oscillation amplitude is $\pm 54 \mu\text{m}$, which corresponds to $\pm 3.3 \%$ as compared to the averaged bubble diameter $a = 1.63 \text{ mm}$. When the bubble is oscillated, the average bubble diameter is 2% larger than the initial size because it spreads out a little bit. In the mean time, at the frequencies of 3.5 and 4.4 kHz, the oscillation amplitude is much smaller than that at the resonance frequency at 4.0 kHz. In addition, the oscillation mode is not surface wave mode but close to the axisymmetric mode.

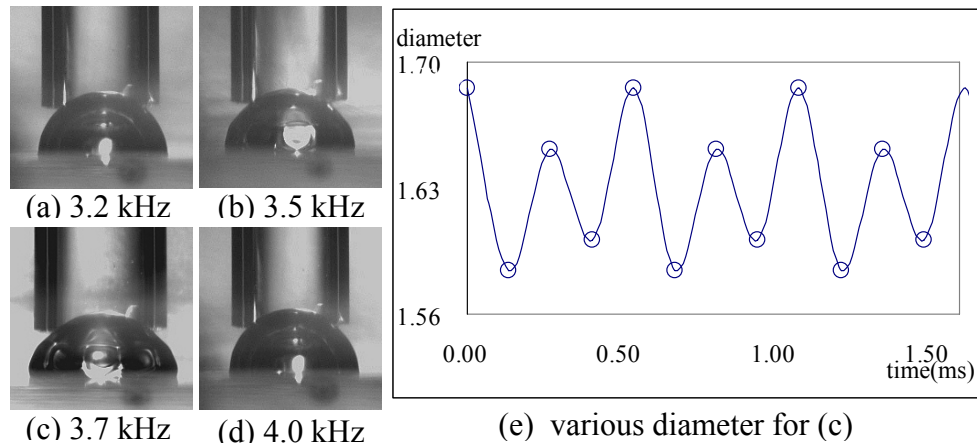


Figure 4 The bubble ($a = 1.6 \text{ mm}$) with the tube installed is excited at four different actuation frequencies of (a) 3.2, (b) 3.5, (c) 3.7 and (d) 4.0 kHz. (e) oscillating diameter in time domain at 3.7 kHz.

When a tube is placed above the bubble, it is observed that the resonant frequency of the bubble becomes lower than the case without the tube. It means that the tube installation disturbs the bubble oscillation. Figure 4 shows that the bubble oscillates with a tube at four different actuation frequency, 3.2, 3.5, 3.7, and 4.0 kHz. The maximum oscillation is shown at the frequency of 3.7 kHz, which is lower than the resonance frequency (4.0 kHz) without the tube.

More interestingly, the major frequency component in the bubble oscillation is twice larger than the actuation frequency, which means that the bubble is oscillating most prominently at the first harmonic. However, similar to the previous case without the tube, the oscillation amplitude is measured at $\pm 54 \mu\text{m}$ ($\pm 3.3\%$ compared to the average bubble diameter, 1.63 mm).

2.3.2 Zero flow rate state

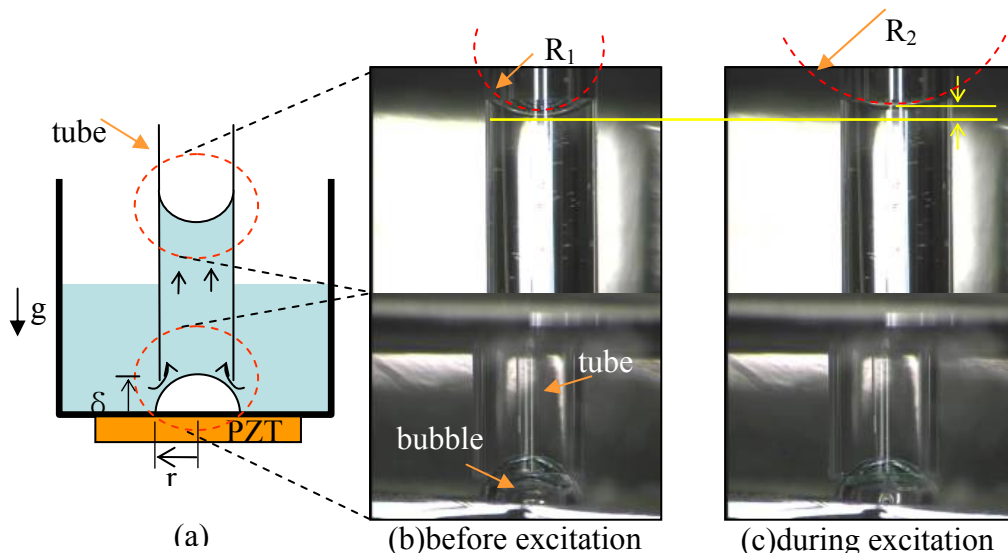


Figure 5 Pressure generation by the oscillating bubble. Since there is no flow in the tube, this represent the zero-flow rate condition (a) Experimental setup of bubble pump. A straight capillary tube is placed vertically above the oscillating bubble to collect upward flows in the cavitation microstreaming. (b) Before acoustic excitation. (c) During acoustic excitation, the curvature of the top meniscus in the tube decreases with a slight increase in water height, showing the excited bubble generating the pressure.

In order to know how much the pressure can be generated by the oscillating bubble, the maximum pressure is measured at the zero-flow rate condition in the tube. As shown in Figure 5, the inlet of a straight capillary tube (inner diameter D is 1 mm) is located above the bubble (the

distance between the inlet and the substrate surface δ is 0.6 mm and the bubble base diameter r is 1.5 mm) in water, while the tube outlet is exposed to the atmosphere (Figure 5a). When the bubble oscillation is turned off, the capillary rise due to the hydrophilicity of the inner wall is measured at 15 mm (the height is balanced by surface tension at the contact line according to Eq. (2)). When the bubble is oscillated at the resonance frequency (4 kHz) (Figure 5b, c), the change in the meniscus curvature at the tube outlet and a slight rise (0.12 mm) of the water level in the tube are observed. Since in this configuration the flow rate in the tube is zero, it can be assumed that the weight of the water in the tube is balanced by the sum of Laplace pressure and the pressure generated by the bubble oscillation (Eq. (3)).

$$\rho g h_1 = \gamma \frac{2}{R_1} \quad (2)$$

$$\rho g h_2 = \gamma \frac{2}{R_2} + \Delta P \quad (3)$$

(γ = surface tension of water, ρ = density, g = gravity)

Equating (2) and (3) yields as

$$\Delta P = \gamma \left(\frac{2}{R_1} - \frac{2}{R_2} \right) + \rho g (h_2 - h_1) \quad (4)$$

By measuring the change in the water level ($\Delta h = h_2 - h_1$) and the radii of the meniscus (R_1, R_2), the maximum pressure generated by the oscillating bubble is inferred. The surface tension of water (γ) is 0.0728 N/m at 20°C. The initial radius of the top meniscus is 0.65 mm (R_1) with the contact angle of 40°, but the radius changes to 1 mm (R_2) with the contact angle of 60° under excitation. The pressure generation of 79.7 Pa largely comes from the Laplace

pressure in equation (4) as compared to the height rise. When taking into account the pinning effect at the contact line of the meniscus, the generating pressure may be estimated higher.

2.3.3 Pumping by oscillating bubble

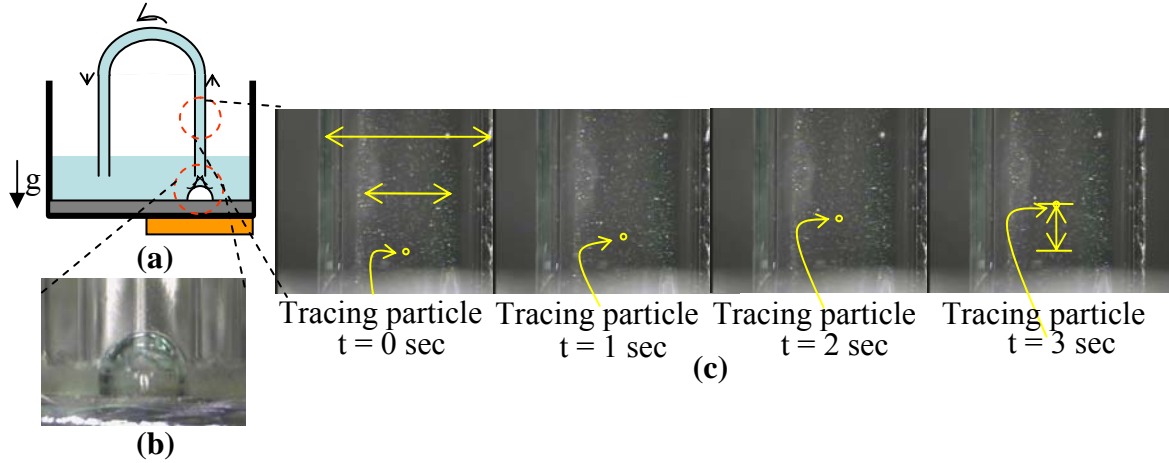


Figure 6 Flow generation by bubble pump (a) Experimental setup of bubble pump. The inlet of the U-tube is placed above the oscillating bubble while the outlet is immersed in the water reservoir. (b) Configuration of the tube inlet and bubble. The bubble diameter is 1.6 mm and the tube inner diameter is 1.5 mm. (c) Particle are seeded and traced to measure the flow velocity and the flow rate in the tube. The measured flow rate in the tube is 0.24 $\mu\text{l/s}$.

To see the pumping, the tube outlet is connected to the water reservoir using a capillary U-type (10 cm) tube (Figure 6a) with one end placed above the oscillating bubble. Note in this configuration that both ends of the U tube are immersed in the same reservoir. For flow visualization in the tube, the microparticles are seeded. From sequential images of tracing particles in Figure 6c, it is evident that the oscillating bubble pumps the liquid through the capillary tube. Based on the particle speed, the Reynolds number of the tube flow is 0.6 at which the flow downstream of the entrance length ($0.0375 D$) would be a *fully developed Poiseuille flow*.

In this pumping configuration, many parameters such as the tube diameter D and the distance δ come into play on the flow rate.

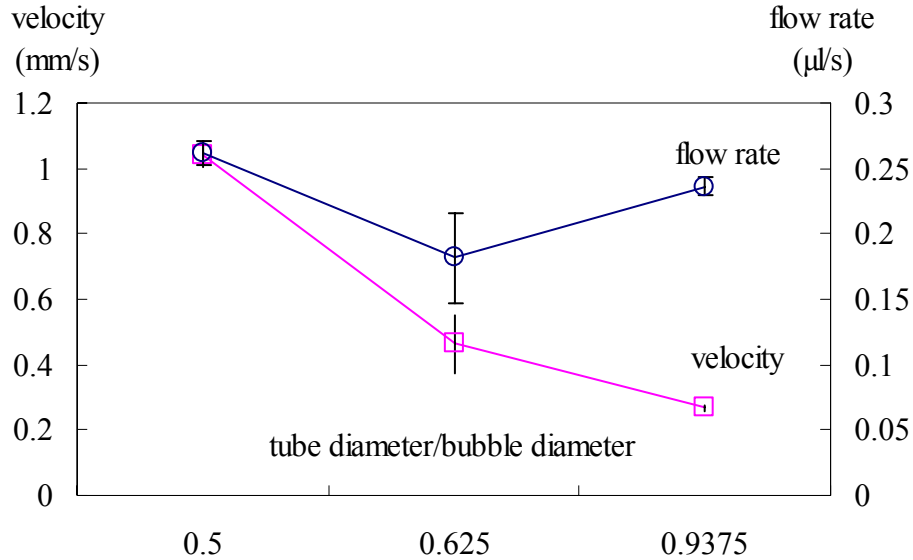


Figure 7 The effect of the inner diameter of the tube on velocity and flow rate. In all cases, bubbles are in contact with the tube inlet rim.

Figure 7 shows the flow rate (velocity) vs. the inner tube diameter, D . The data are averaged from three experiments, and scattering ranges are less than 20%. As D increases, the flow velocity in the tube decreases. This is attributed to the fact that the larger tubes may collect circulating flows in the cavitation microstreaming which do not contribute to the upward flow pumping. As a result, the flow rates are comparable in all three tube diameters, although the pressure resistant for the larger tube diameters becomes smaller. Due to non-availability, experiment with any smaller tubes (smaller than 0.8 mm) could not be made. However, it is expected that the flow rate with smaller tubes may not be higher than that with the 0.8 mm dia tube since the flow resistant in the smaller tube becomes higher. Therefore, the optimum tube diameter in terms of the flow velocity is expected to be about the half size of the bubble.

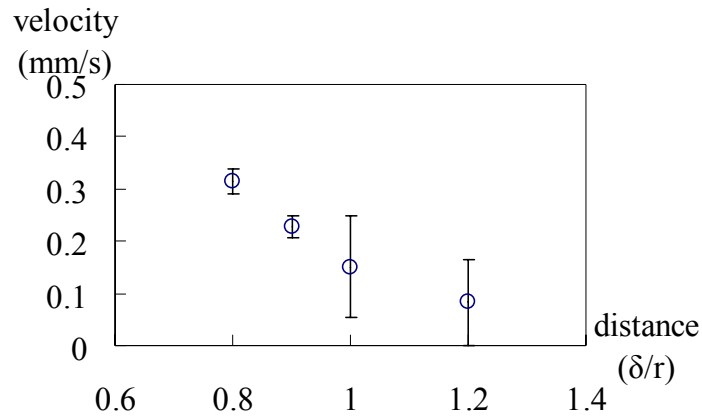


Figure 8 The effect of the vertical position of the tube inlet (δ/r) on the velocity. When $\delta/r = 0.8$ (the bubble is in contact with the tube rim), the velocity is maximum

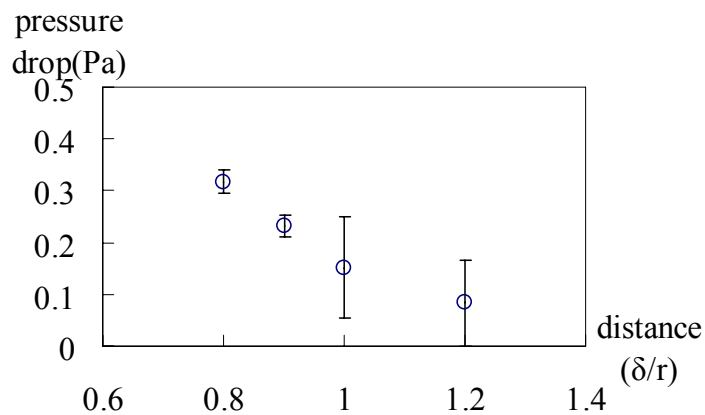


Figure 9 Pressure drop in the tube. The data are reproduced from Figure 8 based on the Poiseuille flow assumption in the U tube.

The effect of the distance δ (defined as the distance between the substrate and tube inlet) on the flow velocity is also studied (Figure 8). As the distance δ increases, the velocity monotonically decreases. The flow rate is quite sensitive to the distance δ . The assumption of the Poiseuille flow in the tube allows us to calculate the pressure drop at the measured velocity, as shown in figure 9. The pressure drop is also monotonically decreases as the distance δ increases.

When the bubble is in contact with the tube rim, the velocity as well as the pressure generation becomes maximized. The data presented are averaged from three different experiments.

2.3.4 Dependence of flow rate on the back pressure

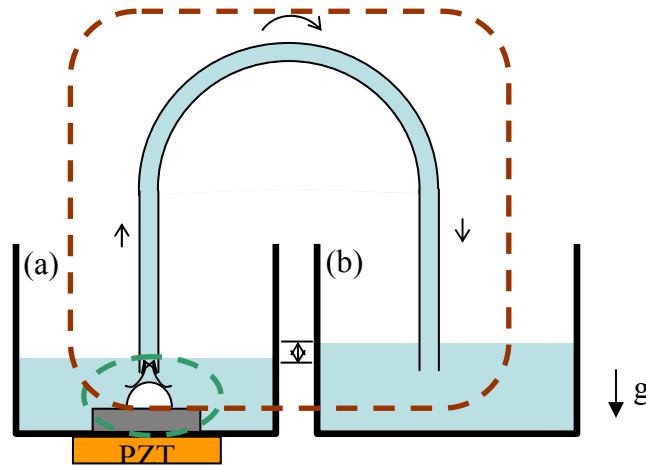


Figure 10 Micropump configuration

To study the dependence of the flow rate on the downstream pressure load, the downstream pressure should be precisely controlled within the pressure the present micropump can generate. However, since the present generated pressure is not high, it is not practically easy to precisely change the pressure load in the downstream. So, a new method is devised to continuously change the downstream pressure load with the entire span of the maximum pressure the micropump can generate. As shown in Fig. 10, the capillary U-type tube, of which two ends are immersed in two reservoirs respectively, is used. The bubble is placed underneath the left end (inlet) of the U tube while the right end (outlet) is open to the water in the reservoir. Once water manually fills the U tube and thus the water column connects the two reservoirs before bubble excitation, the water levels at both reservoirs are automatically adjusted and become equal due to the gravity. The

excitation frequency is set to get the maximum flow rate after aligning the inlet of the tube with a bubble. As the bubble is excited, the water level of the left reservoir becomes lower while the water level of the right reservoir becomes higher because the oscillating bubble pumps the water from the left reservoir to the right reservoir. As time goes on, the flow rate in the tube decreases due to the higher water level in the right reservoir, in other words, higher pressure load in the downstream. Finally, the flow stops when the pressure load becomes equal to the maximum pressure the oscillating bubble can generate. As a result, the bubble pump is loaded under a continuously changing back pressure condition. In this process, by measuring the flow rate, the dependence of the flow rate on the back pressure can be obtained. When the bubble excitation is turned off, the flow is reversed (i.e., the flow returns from the right back to the left reservoir), and the water levels in both reservoirs are equalized. The testing conditions are that the inner diameter of capillary tube D is 1.5 mm, the bubble base diameter r is 1.8 mm, the applied excitation frequency is 2.7 kHz, the length of the tube is 12 cm, and the distance between the inlet and the substrate surface δ is 0.6 mm.

The dependence of the flow rate on the water level difference is shown in Fig. 11. The bubble of 1.8 mm in diameter oscillates at 2.7 kHz, and the cross section of the reservoirs is $29 \times 66 \text{ mm}^2$. Time integration of the flow rate measured from the tracing particle provides the total volume which is pumped from the left to right reservoirs. The water level difference between the reservoirs can be inferred from the total volume. As a result, the back pressure load by the water level difference can be calculated. Initially the flow rate is maximum, close to $\sim 0.7 \mu\text{l}$. As time goes on, the water level pressure increases with decrease in the flow rate. It takes approximately 7 to 10 minutes until the flow rate becomes zero. The trend in Fig. 11 is very similar to the performance curve of other type pumps.

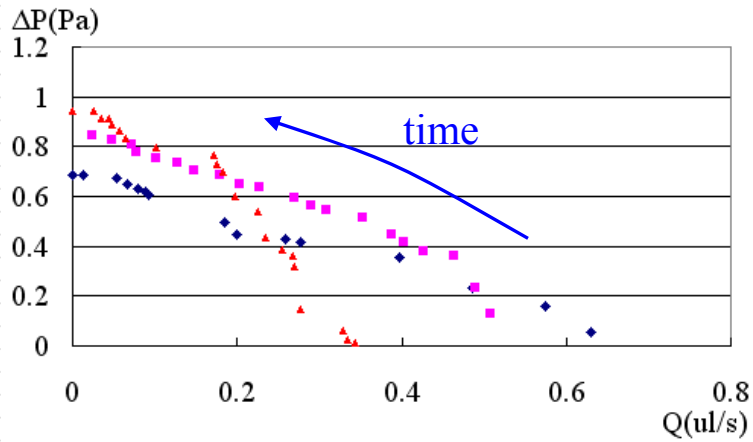


Figure 11 Dependence of the flow rate on the water level difference between the left and right reservoirs

In addition, using the fully developed flow assumption, the flow rate at the instantaneous time allows calculating of the pressure drop in the tube. This pressure drop should be added to the total back pressure load if one may want to regard only the bubble and tube inlet as the pump body. In this case, the pressure drop acts as the back pressure load as well. As a result, the water level difference and pressure drop contribute to the total pressure load as described in equation (5).

$$\begin{aligned}\Delta P &= \Delta P_{\text{head_difference}} + \Delta P_{\text{loss}} \\ &= \rho g \Delta h + \frac{32\eta l v}{D^2}\end{aligned}\quad (5)$$

(ρ = density, g = gravity, h = height, η =viscosity, L = tube length, V =velocity, D =hydraulic diameter). The pressure loss ΔP_{loss} by friction on the inside wall of the tube inside would be inferred based on the Poiseuille flow since the Reynolds number of this flow is less than 1.

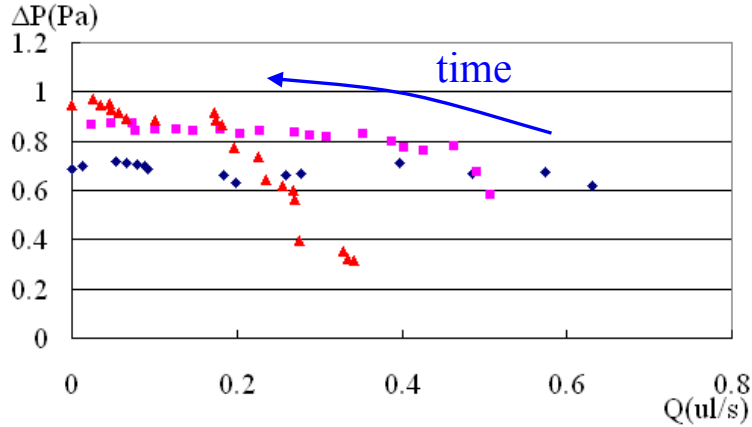


Figure 12 Total pressure load vs. flow rate (draw an arrow indicating time).

Figure 12 shows the total pressure load pressure vs. the flow rate. Unlike the trend in Fig. 11, the total pressure load is maintained nearly constant over the tested flow rate. This is because the trends of pressure drop in the tube and water level difference are opposite, canceling their contributions over the testing flow rate range. That is, at the high flow rate the pressure drop is the major contribution while the water level difference is negligible; at the low flow rate, vice versa.

Although it cannot be measured accurately, the effect of contact line pinning on the reservoir walls should not be overlooked. Due to the contact angle hysteresis, the additional pressure is required to advance the contact line on the right reservoir wall and to recede the contact line on the left reservoir wall (Fig. 13). Taking into account this effect, the additional pressure load for various contact angles can be estimated using the Young-Laplace equation. The pressure difference across the water and air interface can be expressed by the Young-Laplace equation as:

$$dA \cdot \Delta P = \gamma \cos \theta dL \quad (6)$$

where A is the cross section area of the reservoirs, P is the pressure, γ is the surface tension, L is the perimeter of the reservoirs and θ is the contact angle between water and the reservoir.

Setting up Equation (6) for each chamber and subtracting them may yield the pressure resistance induced by contact angle hysteresis as:

$$\delta P = \frac{\gamma(\cos \theta_1 - \cos \theta_2)dL}{dA} \quad (7)$$

For example, if the contact angle on the left reservoir wall is 50° and the contact angle on the right reservoir wall is 59° , the additionally required pressure is estimated to be 0.92 Pa , which should be taken into account to the total pressure load. If this pressure is added to the result in Fig. 12, the maximum pressure the bubble can generate is around 1.8 Pa . For other contact angle combinations, the pressure resistance is tabulated in Table 1.

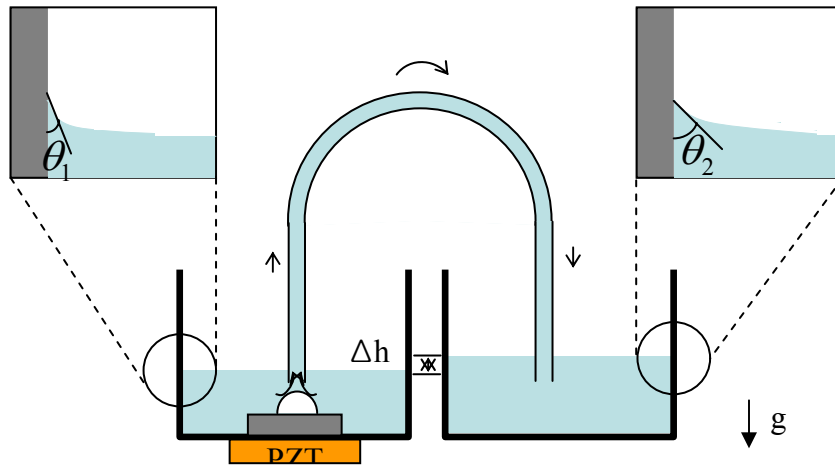


Figure 13 Difference of the contact angles between on the right and left reservoir walls gives an additional pressure load to the bubble pump.

Table 1 Additional pressure load due to the contact angle difference

θ_1 (°)	θ_2 (°)	δP (Pa)
54.5	54.5	0
53.5	55.5	0.21
52.5	56.5	0.41
51.5	57.5	0.61
50	59	0.92

2.4 SUMMARY

When a gaseous bubble is excited by an acoustic wave, it oscillates in harmony with the wave and generates strong vortical flows around it, so-called cavitational microstreaming. In this chapter, a new micropumping method using oscillating bubbles is developed and studied experimentally. The key idea in the pumping method is to install a capillary tube above the oscillating bubble to collect the upward microstreaming flow into the capillary tube.

First, using a high-speed camera, oscillation mode of the bubble is identified as surface mode where the bubble surface undulates with several nodes and antinodes. When the capillary tube is installed on the bubble, the bubble oscillates in the similar surface wave mode, except that the harmonic component is more prominent than other frequency components. The maximum

pressure generated by the oscillating bubble is estimated to be about 2 Pa in the zero-flow condition by measuring the change in the height of rise in the tube and the curvature of meniscus radius in the open end of the capillary tube. The effects of the capillary diameter and the distance between the bubble and capillary inlet on the flow rate and pressure generation are parametrically studied. The velocity and pressure generation monotonically decrease as the tube diameter and the distance increase.

To characterize the dependence of the pumping flow rate on the back pressure load, the downstream back pressure is continuously changed using two reservoirs which are connected through a U type capillary tube. One end of the U tube is placed above the oscillating bubble in the first reservoir while the other end of the U tube is open and immersed in the second reservoir. As water is pumped by the oscillating bubble, the water level in the first reservoir lowers while the water level in the second reservoir rises. As a result, the oscillating pump experiences the continuously increasing back pressure during pumping. By measuring and integrating the flow rate in the tube, the water level difference and thus back pressure are inferred. It is shown that the dependence of the flow rate on the back pressure load is very similar to conventional performance curves of other type pumps. However, the present testing system involves the pressure drop throughout the tube and additional frictions on the reservoir walls that also significantly contribute to the total back pressure load. When taking into account these loads, the present micropump can reach the flow rate of $\sim 0.7 \mu\text{l/s}$ and the pressure generation of $\sim 2 \text{ Pa}$. As a result, the present pump can be classified into the large-flow-rate and low-pressure type pump.

The present pumping principle requires neither mechanical moving parts nor complex wiring for signal and power inputs, implicating potential applications in many implantable microfluidic devices such as drug releasing/dosing pump. To run the pump, the currently existing

ultrasonic transducers can be readily used to remotely excite the bubbles in the pump without any physical or electrical connections.

2.5 FUTURE WORK

In this chapter, it is proven that oscillating bubbles can be used as a pumping source. However, more detailed physical understanding is currently missing. Even the flow field around the bubble oscillating in surface wave mode without the capillary tube is not clearly understood yet. To my knowledge, there have not been any experimental or theoretical studies on the cavitation streaming flows induced by surface-wave-mode oscillating bubbles. Furthermore, it is expected that when the capillary tube is placed over the bubble, the detailed flow field around the oscillating bubble becomes more complicated. In order to understand flow dynamics and to optimize the pumping conditions, measurements of the flow field should be made in the near future. In order to correctly measure the flow field, the measurement system should be non-invasive. Otherwise, the invasive physical probe may completely change the flow field. For this purpose, one of the best candidates would be the microPIV (particle image velocimetry) system. By taking two consecutive images of seeded particles in the cross section, the entire flow field on the section can be acquired in a single measurement. Along with the microPIV measurements, numerical modeling and simulation will provide more information in the flow field such as pressure field. Numerical results can be verified against experimental results and thus be corrected. These complimentary approaches possibly elucidate the detailed physical mechanisms of cavitation microstreaming flow and its pumping effect in the present configurations.

3.0 SEPARATION AND COLLECTION OF MICROPARTICLES USING OSCILLATING BUBBLES

3.1 BACKGROUND

Manipulation of individual objects including transporting [59], mixing/reacting [32], separating [60], and trapping is a great concern and challenging issue in biomedical applications [61, 62]. For these applications, various methods have been developed. Among many, micropipetting is the most commonly-used method[61, 62]. However, some disadvantages of this method are that it is likely to generate physical damages on the objects due to direct contact, and it is difficult to integrate with microfluidic systems due to many bulky moving parts required. As alternatives, non-contact manipulating techniques have been developed. Examples include the optical tweezers [63, 64], the dielectrophoretic trapping method [65, 66], the acoustical tweezers[67, 68], and so on.

In the previous chapter, it is shown that oscillating bubbles are used as a fluid pumping actuator. Recently, in our group, it is discovered that acoustically-excited oscillating bubbles provide an additional functionality. The objects [27] neighboring the oscillating bubble are attracted and captured by the bubble. More interestingly, the capturing behavior is dependent on the object size. For example, as shown in Figure 14 a-2 and b-2, 80 μm glass particles are collected to the bubble rim whereas 8 μm particles are repelled away from the bubbles after

applying acoustic excitation on the bubbles for seconds. Note that particles of the two different sizes are initially mixed and deposited on the surface. It is found that only large particles (typically $> 20 \mu\text{m}$) are attracted to the bubble surface while small particles are repelled from the oscillating bubble drifting into the surrounding vortical streamlines. In this chapter, this phenomenon is exploited for microfluidic applications to separate and collect particles by size in the micro channels and chamber.

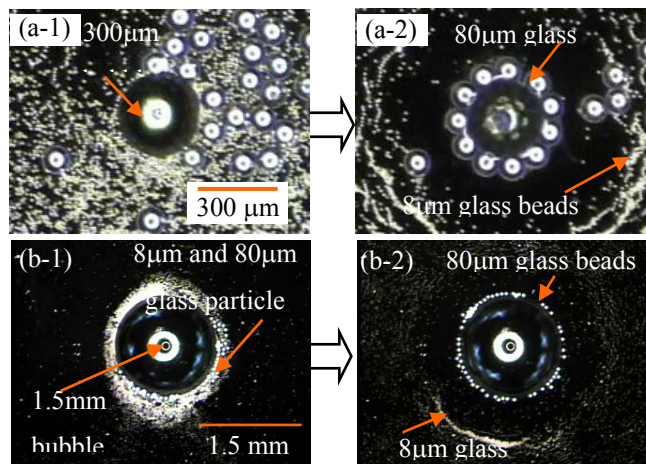
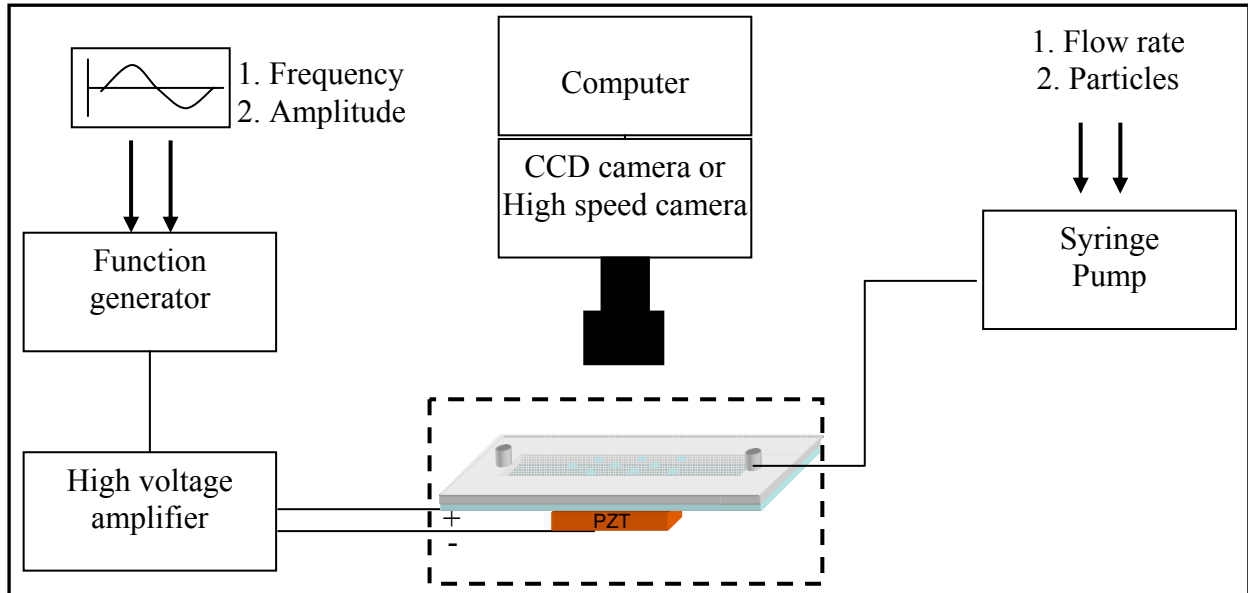


Figure 14 Sequential pictures showing that acoustically excited oscillating bubbles can separate particles of two different sizes. (a) with a $300 \mu\text{m}$ bubble and mixtures of $8 \mu\text{m}$ and $80 \mu\text{m}$ glass particles: (a-1) initial state; (a-2) After acoustic excitation, most of the $80 \mu\text{m}$ particles are collected near the bubble whereas the $8 \mu\text{m}$ particles are repelled away; (b) with a 1.5 mm bubble and mixtures of $8 \mu\text{m}$ and $80 \mu\text{m}$ glass particles: (b-1) initial state; (b-2) After acoustic excitation, the $80 \mu\text{m}$ particles are collected around the bubble whereas the $8 \mu\text{m}$ particles are repelled away.

3.2 EXPERIMENTAL SETUP



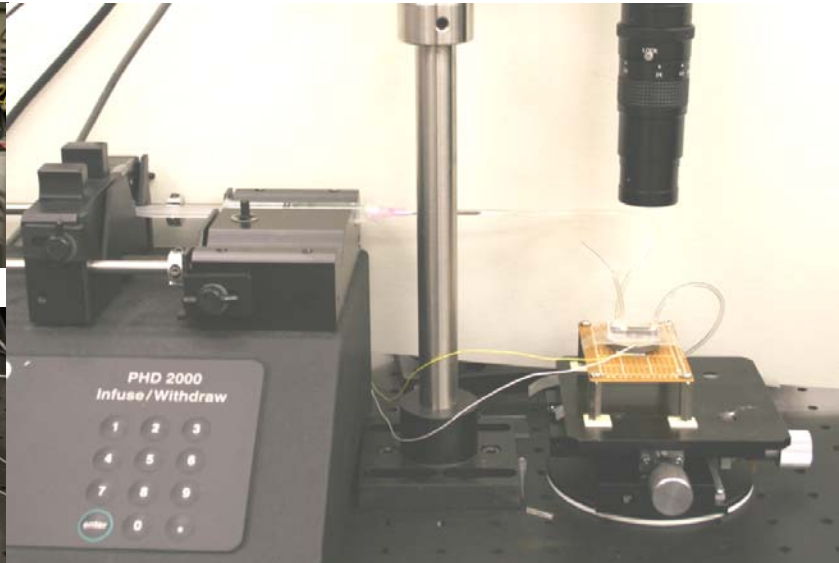
(a)



(b)



(c)



(d)

Figure 15 Experimental setup for particle separation and collection with fluidic devices (a) experimental schematic diagram (b) function generator and power amplifier (c) syringe pump (d) microscope, and syringe pump

To evaluate the separation behavior for microfluidic applications, three different kinds of fluidic testing devices are fabricated: two are channel type (mini and micro scales) and the other is the chamber type. All the three fluidic devices use oscillating air bubbles as particle collecting source. As shown in Figure 15, for bubble excitation, the fluidic device is directly glued to a bulk piezo transducer (ring shaped 20mm diameter). Sine waves are generated by a function generator, amplified by a high voltage power amplifier, and transmitted to the piezo actuator. The applied frequency ranges from 10 kHz to 30 kHz, which corresponds to the bubble resonance frequencies. Since the frequency is relatively low compared to the device size, the bubbles are exposed to homogeneous acoustic fields without nodes and antinodes. The objective of these experiments is both separating and capturing 80 μm particles from smaller particles (e.g., 10 μm , and 2 μm particles). Tested particles are glass or polystyrene particles all purchased from Duke scientific Corp.

3.2.1 Particle separation and collection in a minichannel

The conceptual drawing of minichannel for particle separation and collection is shown in Figure 16a. Single or multiple bubble(s) are located on the bottom of the minichannel. The bubbles are excited by the PZT and oscillate at their resonance frequency. Initially a mixture solution of larger and smaller particles is injected through the minichannel using a syringe pump (PHD2000, Harvard Apparatus). When the bubble starts to oscillate, the larger particles laden in the flow are trapped by the oscillating bubbles while the smaller particles are advected downstream passing the bubbles. To hold the bubbles in place against the flow, a hydrophobic Teflon-layer is coated on the channel bottom surface and patterned to the bubble base circles.

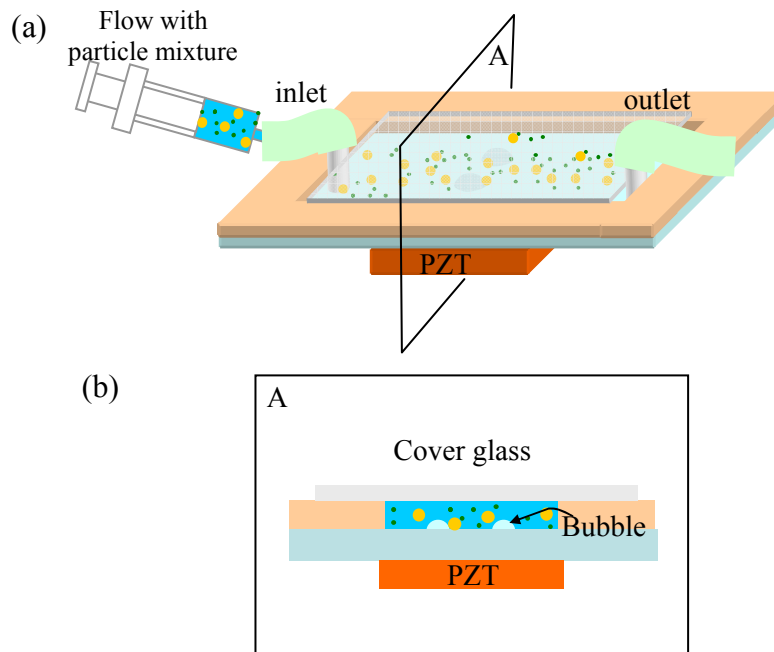


Figure 16 (a) Perspective view of minichannel configuration for particle separation and collection (b) Cross section view. The channel dimension is 15 mm (L) x 2.4 mm (W) x 1.5 mm (H). Water flow with a mixture of 80 μm glass particles and 10 μm polymer particles is injected by a syringe pump at 0.3 ml/min (average speed of 1.4 mm/sec). The bubbles in the minichannel oscillated with the PZT actuator, so they trap large particles laden in the flow.

Figure 17 illustrates fabrication steps of the minichannel. The glass substrate is cleaned using a piranha solution (mixture of sulfuric acid (SiO_2) and hydrogen peroxide (H_2O_2)), and is spin-coated with a 2%-Teflon solution. To enhance the adhesion between the Teflon layer and glass substrate, two steps of annealing at 250°C and 330°C are carried out for 5 min and 20 min, respectively. To pattern the Teflon layer, the Photo resist (AZ4210) solution mixed with fluorosurfactant is spin-coated [69]. After photolithography and reactive ion etching processes, a circular Teflon layer is formed on the glass substrate. Since the Teflon layer is hydrophobic, the bubbles are expected to be trapped on the circular Teflon patterns when the channel is initially

filled with water. However, it turns out that this bubble trapping is not reliable. Furthermore, the size of the trapped bubbles is not exactly the same as the Teflon pattern in many cases. The trapping behavior is highly dependent on many parameters such as the height of channel and the flow speed, etc. The trapping process is not very controllable. Therefore, in some experiments, the air is directly injected on the Teflon patterns by a volume controllable micropipette. Although this method is not automatic, the injected bubble is confined on the Teflon circles with the nearly same size as the Teflon circles.

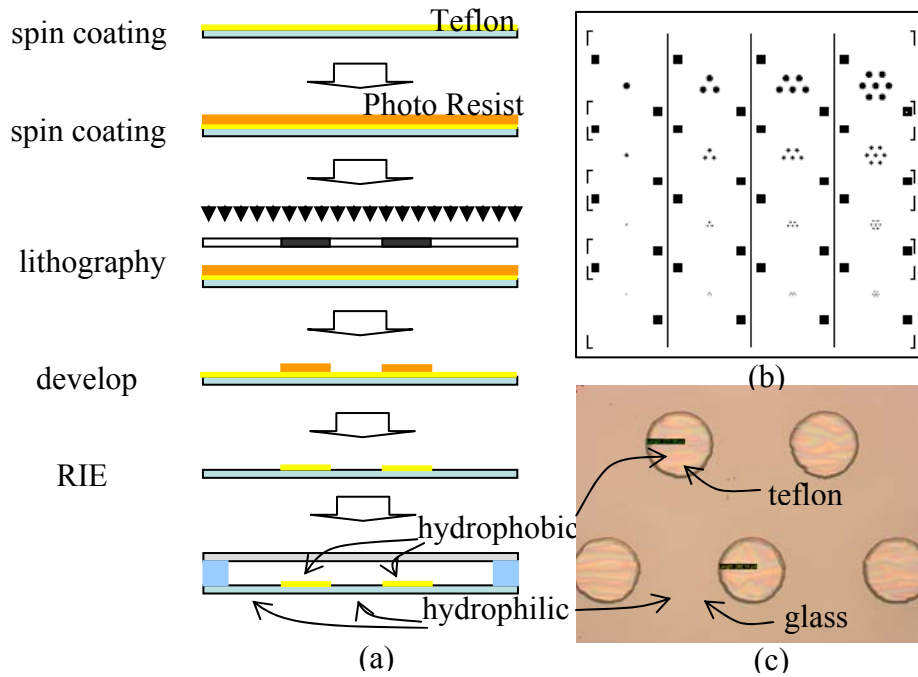


Figure 17 (a) Microfabrication steps of minichannel. 2% Teflon solution is spin-coated and annealed on a glass substrate. A mixture solution of AZ 4210 and fluorosurfactant is spin-coated. After the photolithography process and the reactive ion etching process, the Teflon layer is patterned into the circles (b) Mask design. The circle diameters are 1 mm, 0.75 mm, 0.5 mm, and 0.25 mm. (c) Teflon-patterned glass substrate. The bare glass parts are hydrophilic while the Teflon circles are hydrophobic.

Figure 18 shows that a 330- μm -diameter bubble excited at 19 kHz (100 V) traps 80- μm particles laden in the flow (Figure 18b-d), while 10- μm particles pass the bubble as many blurred particle pathlines are shown in Fig. 18c. The trapped large particles are collected on the bubble surface. The average flow speed is 1.4 mm/s. Upon turning off the PZT actuator, the trapped large particles are released from the bubble and moving downstream by the flow (Figure 18e and f).

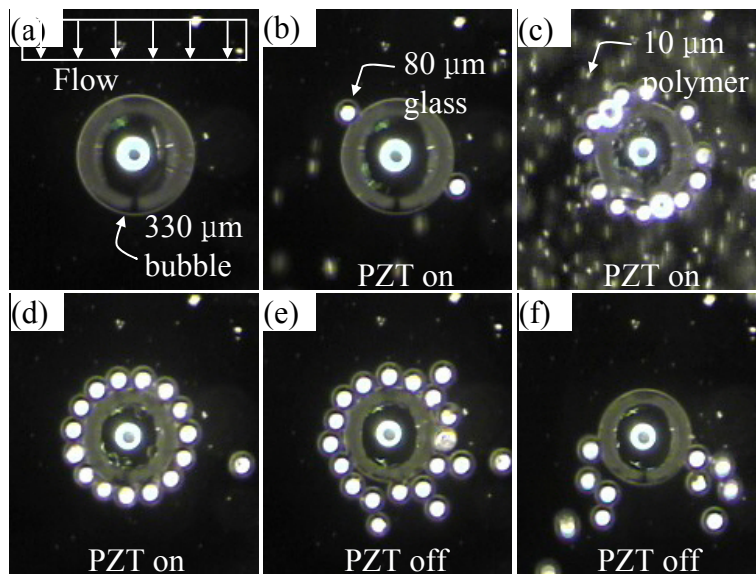


Figure 18 Single bubble case in minichannel: A single bubble (diameter is 330 μm) oscillates under acoustic excitation at 19 kHz, trapping only 80- μm particles, not 10- μm particles. (a) initial condition (b)-(c) 10- μm particles pass the oscillating bubble while 80- μm particles are trapped by the oscillating bubble. (d) 10- μm particles are washed away. (e-f) Upon the PZT actuator off, 80- μm particles are released and advected downstream by the flow.

Similarly, two adjacent bubbles of 250- μm diameter that are laterally placed next to each other at a distance of 750 μm in the minichannel are examined (Figure 19a). The bubbles are located 2 mm downstream of the channel entrance. Since the two bubbles are the same in size, their resonance frequency is also the same at 24 kHz. The number of trapped particles is much higher than the single bubble case (Figure 19c and d). No large particles are seen to pass between the bubbles without being trapped until holding capacity of the bubble seems to be reached to the limit.

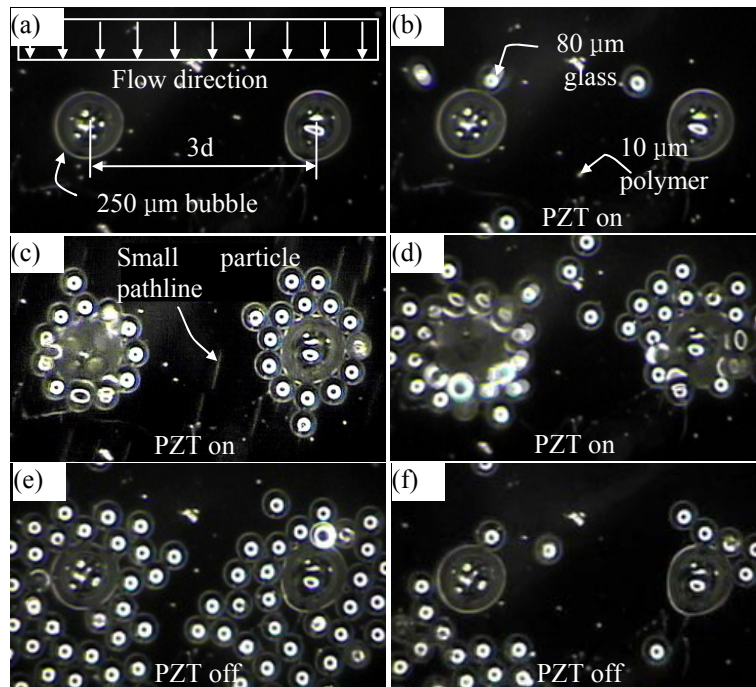


Figure 19 Two bubbles (250 μm dia.) of the same size are excited at 24 kHz. The bubbles are located in the middle of the channel. (a) initial state. (b)-(c) 8- μm particles pass the oscillating bubbles while 80- μm particles are trapped by the oscillating bubbles. No particles of 80- μm are seen to pass between the bubbles. (d) 8- μm particles are washed away. (e-f) Upon the PZT actuator off, 80- μm particles are released and advected downstream by the flow. The number of trapped particles is much larger than the single bubble case.

3.2.2 Particle separation and collection in a microchannel with cavities

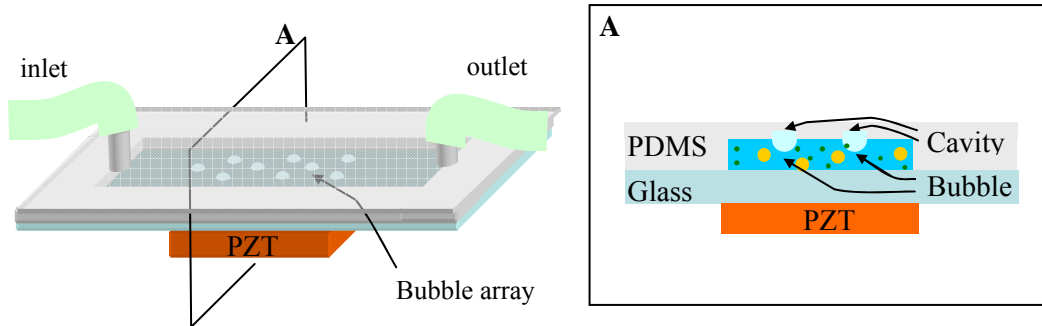


Figure 20 (a) Configuration of collection and separation in a microchannel with cavity; (b) Cross section view. The channel dimension is 15 mm (L) x 1.5 mm (W) x 0.125 mm (H). Cavities form on the PDMS structure. Water flow with a mixture of 80 c and 2 μm glass particles is supplied by a syringe pump at 0.1 ml/min (average speed of 9 mm/sec). The bubbles in the microchannel are oscillated by the PZT actuator, trapping large particles laden in the flow.

In the previous minichannel design, the bubbles are manually deposited using a micropipette. This may hamper realizing automated microfluidic devices. In order to obviate this problem, the channel type device is modified for improved bubble deposition. As shown in Figure 20, the key modification is that the channel has micro cavities on the top plate rather than the patterned Teflon circles to automatically deposit and hold bubbles against the flow in the channel. Also note that the channel is in the microscale, much smaller than the previous design. An array of cavities is formed in the PDMS replica that serves as the top plate in the microchannel. In this design, it is expected that water is pinned at the rim of the cavities and thus microbubbles, of which base diameter is exactly the same as the cavity diameter, are trapped on the cavities when the microchannel is primed.

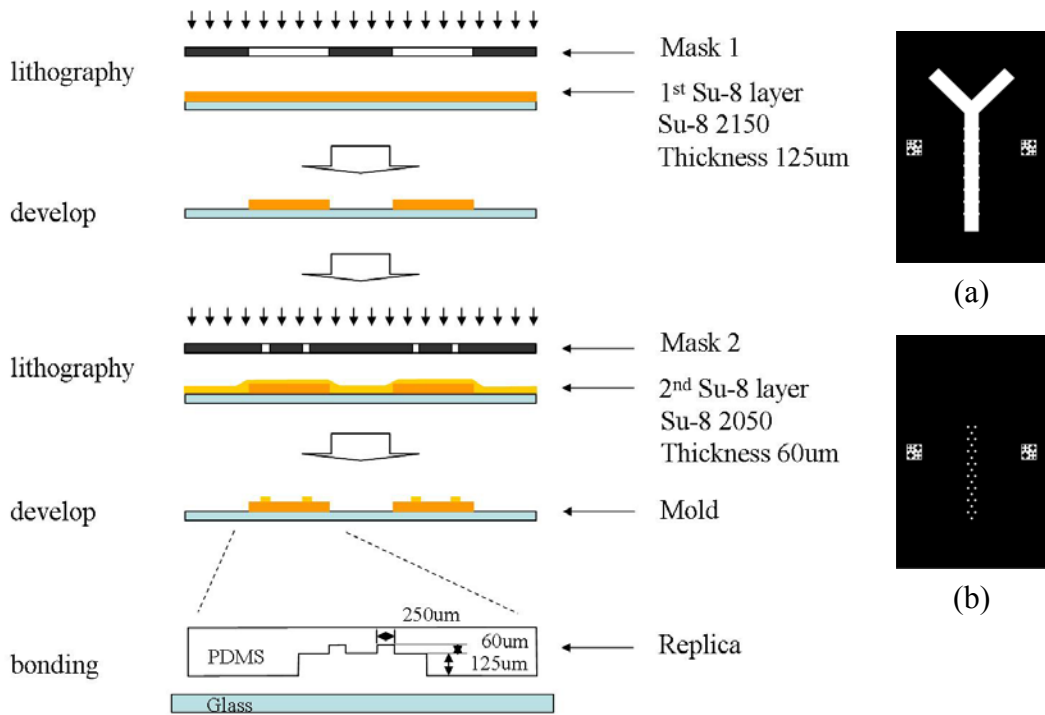


Figure 21 Fabrication steps of particle separating/capturing in a channel with cavities. (a) negative photo mask for the channel (b) negative photo mask for the cavities

Figure 21 depicts detailed fabrication steps of the modified microchannel design with microcavities. The key process involves soft lithography where micro cavities are replicated in the transparent PDMS (Polydimethylsiloxane) material. The overall fabrication process consists of three steps: (1) build a mold, (2) form a replica, and (3) bond the replica to a glass substrate. To build the step-shaped mold, two photolithographic processes are repeated. The SU-8 (negative photoresist) photoresist solution is spin-coated on a Si substrate, resulting in a SU-layer of 125 μm in thickness. The SU-8 layer is patterned into the mold of the microchannel. The SU-8 thickness eventually determines the microchannel height. After the first photolithography process, the second lithography with a 60 μm thickness SU-8 layer is spin-coated on the top of the microchannel mold and patterned into the mold of the microcavities. In this process, the

cavity patterns should be precisely aligned with the first microchannel pattern. A mixture solution (10:1) of liquid silicone rubber base and curing agent (sylgard 182, Dow Corning) is degassed, poured over the master mold, and heated. Finally, it becomes a transparent solid PDMS elastomer after detaching the master mold. The final step is to bond the PDMS replica with a glass substrate. For the irreversible bonding process, the surfaces of the PDMS replica and glass substrate are treated in the air plasma for 30 seconds [70]. This treatment produces the appropriate interfacial interactions. For more detailed fabrication process, see Xia et al [71].

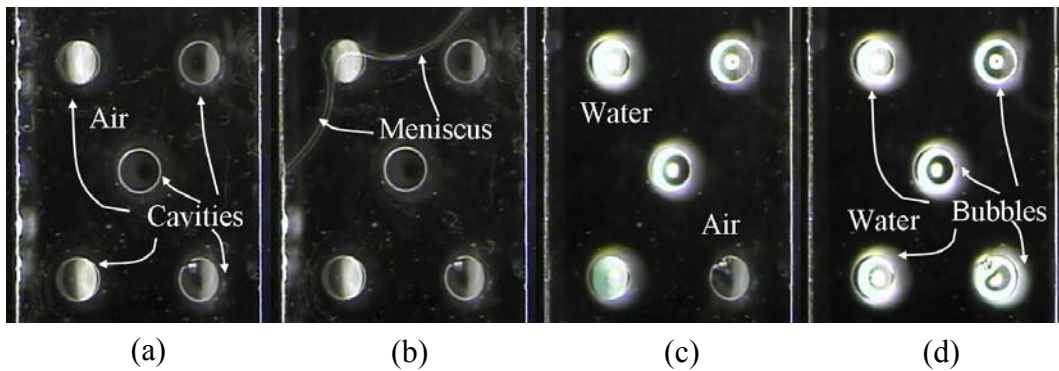


Figure 22 Sequential images of automatic bubble deposition on cavities in the microchannel.

Figure 22 shows the sequential images of how 250- μm -diameter bubbles form in cavities as the microchannel is primed. When water is injected into the microchannel, the leading meniscus advances downstream of the microchannel (figure 22 b and c). Although the water flows over the cavities, they are not filled with water. As a result, bubbles of the cavity size are trapped on every cavity (figure 22d). It is confirmed that this process is highly reliable with reproducibility.

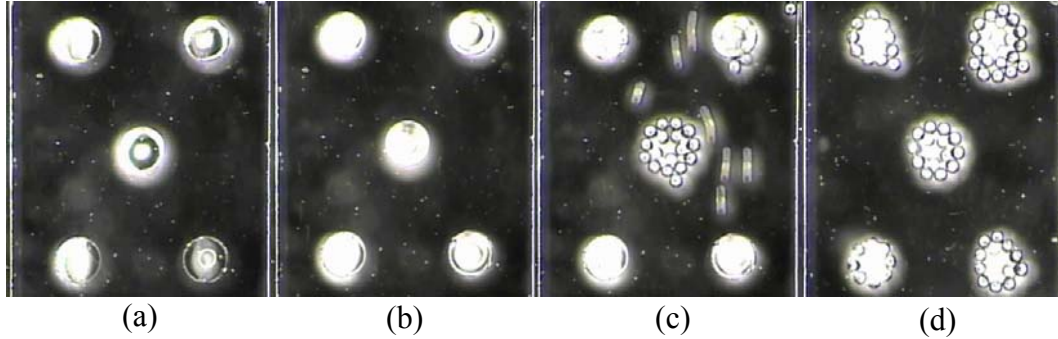


Figure 23 Sequential images of particle capturing and separating in the microchannel with cavities. An array of microbubbles (diameter is $250\ \mu\text{m}$) oscillates under acoustic excitation at 24 kHz. A premixed solution of $80\text{-}\mu\text{m}$ and $2\text{-}\mu\text{m}$ particles is injected into the microchannel. (a) initial condition (b) bubbles are excited at 24 kHz (c), (d) $2\text{-}\mu\text{m}$ particles pass the oscillating bubbles while $80\text{-}\mu\text{m}$ particles are trapped by the oscillating bubbles.

Using the new design of the microchannel with cavities, particles separation and collection behaviors are examined as sequential images of testing results are shown in Figure 23. The bubble size is uniform with $250\ \mu\text{m}$ diameter. An array of microbubbles (diameter is $250\ \mu\text{m}$) oscillates under acoustic excitation at 24 kHz. A premixed solution with $80\text{-}\mu\text{m}$ and $2\text{-}\mu\text{m}$ particles is injected into the microchannel. $80\text{-}\mu\text{m}$ particles are trapped on the oscillating bubbles while the $2\text{-}\mu\text{m}$ particles pass the bubbles. The averaged flow speed is measured to be $9\ \text{mm/s}$. It is roughly estimated that the capturing range of each bubble can reach the distance of the three times bubble radius. Once the upstream bubbles reach the capturing limit in the particle number, it is found that the $80\text{-}\mu\text{m}$ particles pass the upstream saturated bubbles but they all are captured by the downstream oscillating bubbles.

3.2.3 Particle separation and collection in a microchamber using mobile oscillating bubble

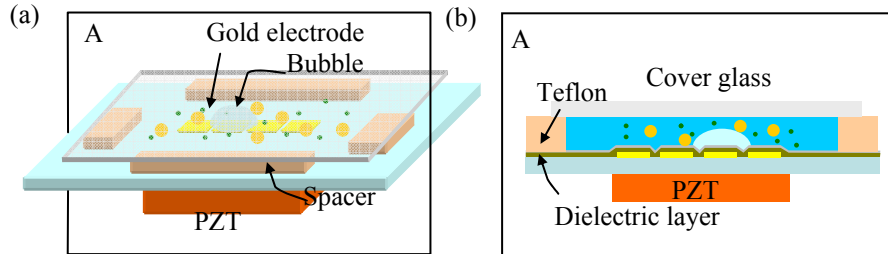


Figure 24 (a) Configuration of collection and separation in a microchamber by a mobile oscillating bubble; (b) Cross-section. The bubble is transported by EWOD and simultaneously excited by the PZT actuator, collecting large particles on its path. Each square electrode is $250\ \mu\text{m} \times 250\ \mu\text{m}$. Applied voltage for EWOD is 80 V. Spacer thickness is $120\ \mu\text{m}$. 8- and $80\text{-}\mu\text{m}$ particles are initially mixed in a water solution.

Another configuration for evaluation of particle separation and collection is a microchamber, as illustrated in Figure 24. Micro bubbles can be moved on a 2-D surface by sequentially activating a square electrode array, so called electrowetting-on-dielectric (EWOD)[72-74]. For more details on EWOD bubble operations, refer to Zhao and Cho [28] and Chung et al [75]. At the same time, the bubble is also oscillated at the near resonance frequency by the PZT actuator, collecting large particles and repelling smaller particles on its path while in lateral motion.

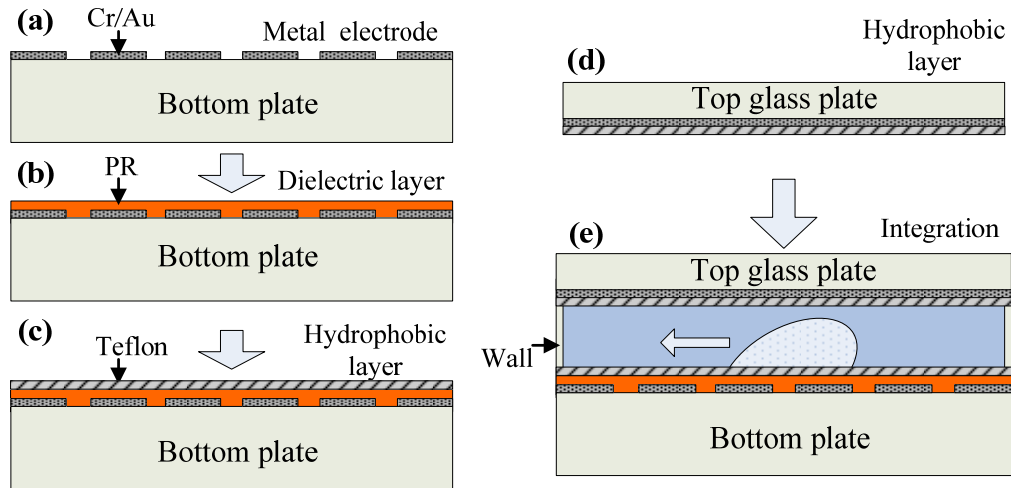


Figure 25 Microfabrication steps of microchamber testing device: (a) Metalizing and patterning of electrodes (Cr/Au) on the bottom plate; (b-c) Depositing of a photoresist as a dielectric layer and a Teflon as hydrophobic layer on the bottom plate; (d) Deposition of a Teflon layer on the top plate (e) Integration of the top and bottom plates with walls in between.

In order to prove this concept, microchamber type testing devices are microfabricated as detailed fabrication steps are illustrated in Figure 25. The microchamber testing devices that consist of two parallel plates (top and bottom) are fabricated using standard lithographic micro fabrication technology. The bottom plate contains an array of EWOD electrodes whereas the top plate is coated with an ITO (Indium Tin Oxide) layer for an EWOD ground electrode. The main fabrication process for the bottom plate consists of three steps: metalizing and patterning of electrodes (Figure 25 a), and depositing of a dielectric layer and a hydrophobic layer (Figure 25 b and c) on the bottom plate respectively. For the EWOD driving, a Au layer of 1500 Å in thickness along with a chromium adhesion layer of 100 Å in thickness is sputter-deposited on a glass wafer and then patterned by wet etching (Figure 25 a). Each EWOD driving electrode is square in shape with side length 250 μm. For the EWOD dielectric layer, a 3-μm thick

photoresist (AZ4210, Clariant Co.) layer is spin-coated on the entire top surface of the bottom plate (Figure 25b). Finally, the bottom plate is coated with a hydrophobic Teflon layer (Figure 25 c). The top glass plate coated with an ITO layer is also spin-coated with the hydrophobic Teflon layer. The transparent ITO layer covering the entire area of the top cover glass makes bubble motions visible.

The last step of the fabrication process is to integrate the two plates as shown in Figure 25e. After putting a large water drop on the bottom plate, the top plate is gently pressed against the walls that are placed on the bottom plate. Multiple layers of double-sided tape (about 100 μm thick each) are used for the walls to confine the water in place and served as spacers. Spacer thickness (120 μm) defines the chamber height and should be large enough to accommodate the target particles of 80 μm in diameter.

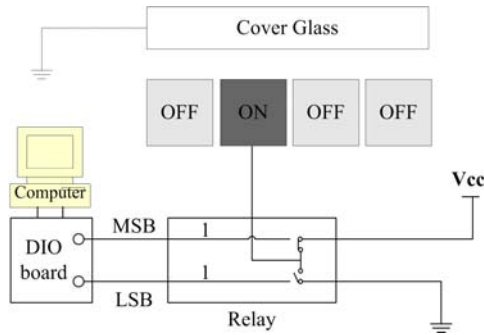


Figure 26 Schematic of activation signal flow for EWOD bubble operation

Figure 26 illustrates how to generate input signals to the EWOD electrodes. The whole system consists of a personal computer, a digital output board (DAQPad-6507, National Instrument), and a custom-made interface circuit mainly containing photo-coupled relays. A PC-based program generates control signals transmitted through the digital I/O board. The control signals switch the relays that provide activation voltages to the electrodes on the testing devices. The applied voltage to the electrodes is set at $V_{cc} = 50 \text{ VAC}$ at 1 kHz.

Testing results are shown in Figure 27. Sequential images show that a 250- μm oscillating bubble is transported step-by-step to the left by EWOD, simultaneously trapping and carrying 80- μm particles; however, 8- μm particles are repelled from the bubble and scattered everywhere. As a result, most of the 80- μm particles are collected in the left side in Fig. 27e/f.

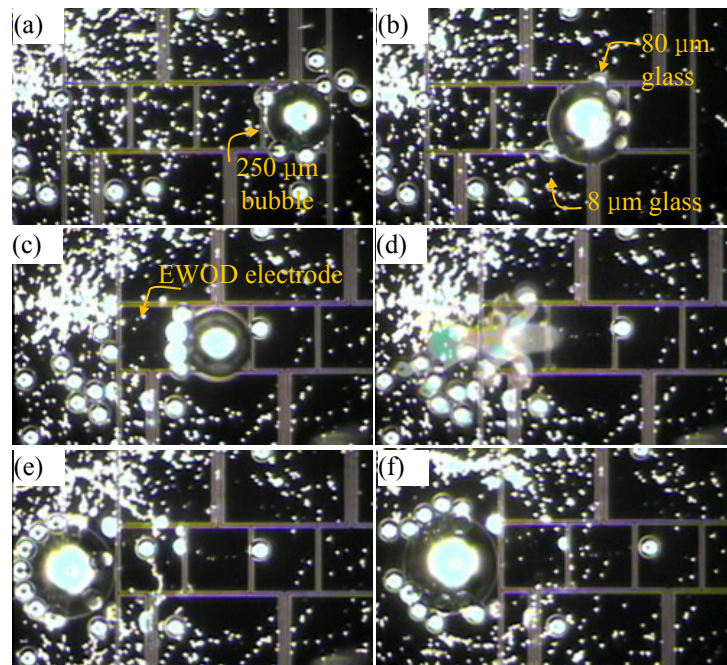


Figure 27 A bubble of 250- μm diameter is transported to the left by EWOD and oscillated by acoustic excitation at 20 kHz (a) initial condition (b-d) The oscillating bubble traps and carry 80- μm particles, not 8- μm particles, while in lateral motion. The bubble loses one 80- μm particle with sudden EWOD moving (e-f) releasing 80- μm particles at the end upon turning off the acoustic excitation.

3.3 SUMMARY

Recently, it is discovered by our group that oscillating bubbles selectively attract and capture large neighboring particles. This chapter studies separation and collection of particles using acoustically-excited oscillating bubbles in three different fluidic configurations; mini- and micro channels with injected flow stream and microchamber with electrowetting-on-dielectric (EWOD) actuated bubbles. To demonstrate the separation and collection, two different sizes (80 μm and 2 μm in diameter) of particles are examined.

First, separation and collection of particles are examined in mini-channel. Since the bubbles are easily washed away by the flow, the bottom surface layer is patterned into Teflon circles on which bubbles are manually deposited. A mixture solution with the two types of particles is injected in the channel inlet using a syringe pump. When the bubbles are excited and oscillated by a piezo transducer, 80- μm particles in the stream are captured by the oscillating bubble while 10 μm particles pass the oscillating bubbles without being captured.

Similar experiments are carried out in a microchannel. A main feature of the microchannel distinct from the minichannel is that it has micro cavities (not Teflon circles) on the top surface to facilitate automatic bubble deposition. When the microchannel is primed with water, the water is pinned at the rim of the cavities (not filling the cavities), resulting in automatic bubble deposition on the cavities. Similarly, when the deposited bubbles are excited, 80- μm particles in the flow stream (9 mm/s) are captured on the oscillating bubbles while 2 μm particles pass the oscillating bubbles without being captured. By simply turning off the acoustic excitation, the captured particles are easily released by the flow stream.

Since the filled water in the microchamber is quiescent, the oscillating bubbles need to move in the chamber to selectively capture large particles suspended in the chamber. 2-D movements of the oscillating bubble are achieved by sequentially activating a square electrode array on the chamber bottom surface, so-called electrowetting-on-dielectric (EWOD). When the bubble is simultaneously actuated by EWOD and acoustic excitation, it captures and carries 80- μm particles, not 2- μm particles.

3.4 FUTURE WORK

In this chapter, although the concept for particle separation is experimentally proven in the three different configurations, there are many questions remained open. The most important question is what the capturing mechanism is. In the past, similar capturing phenomena have been reported. Lutz et al [76] reported the hydrodynamic tweezers in which particles are trapped in the center of vortices formed around the 2-D cylinder. In their works, oscillating flows are applied to the 2-D cylinder fixed in the microchannel. They could not provide explanation on the capturing mechanism either. The main difference from the present configuration is that the excitation frequency is very low (~ 4 kHz). In addition, the boundary condition on the solid cylinder surface is the no-slip condition as opposed to the slip condition on the bubble. Another similar capturing phenomenon is found in Hu et al [77]. In their work, when a vibrating needle is immersed in liquid, particles are captured on the needle tip. Their actuation frequency is very high, one order of magnitude higher than the present condition. They attributed the capturing mechanism to the acoustic radiation force. That is, the particles are collected in the pressure nodes or antinodes. However, in the present configuration, the wave length of the excitation

wave is much larger than the chamber or channel dimensions, which means that the sound pressure is homogenous over the entire dimensions without nodes or antinodes. Most recently, Daniel group [78] reported that hydrophobic polymer pieces are captured near the oscillating bubble. However, they could not explain the mechanism either.

Although the sound pressure is nearly uniform over the channel, the pressure induced by the microstreaming flow may not be uniform but significant enough to move particles. Typically, the pressure minimum occurs in the center of vortices. This is consistent with Lutz's results that the particles are captured in the vortex center. Based on these, it can be speculated that the flow-induced non-uniform pressure acting on the particles may be the main force to attract particles. To confirm this speculation, it is necessary to measure the pressure field. However, this is almost impossible in such a small dimension. One possible way to acquire the pressure field is to use a numerical simulation method. As previously mentioned in the Chapter 2 future work, the numerical method should be first validated with the velocity field measured by the microPIV system. Once the numerical method is validated with accurate models, it can provide information on the pressure field and possibly the resultant force on the particles. These information may answer many questions such as capturing mechanism, dependence of capturing on many parameters such as particle size, bubble size, bubble oscillation amplitude, and so on. Furthermore, the numerical method may provide information on how much force can be generated. In the future, this work should be carried out.

4.0 CONCLUSION

In this thesis, the principle, device fabrication, and experimental proof for two new micro fluidic functions are presented: one is micropumping and the other is microparticle separation. Both fluidic functions are operated based on an oscillating bubble excited by acoustic wave. Fundamental physical principles are related to cavitation microstreaming flows. The key concept for the micropump is to collect upward flows in the cavitation microstreaming flow by putting a capillary tube over the oscillating bubble. In a wide range of testing conditions, this pumping principle is confirmed effective and quantitative measurements of pumping performance are made. This pumping method has potential to create an implantable micropump with no need for wiring or physical connection. However, for better understanding and optimizing the pumping principle, complimentary works of numerical and experimental methods are required in the future.

It is found that oscillating bubbles can capture neighboring objects. This principle is extended to capture particles in microchannels and microchambers. Using microfabricated testing devices, the principle is examined. The results show that the capturing force is strong enough to capture and hold particles advecting in the flow stream in the microchannel. In addition, the capturing is more effective with larger particles, enabling separation of large particles from small particles. This principle is also confirmed effective in the microchamber where electrowetting-on-dielectric (EWOD)-actuated bubbles capture and carry only large

particles suspended in a quiescent medium but not small particles. This principle can be extended to separate biological cells by their size. However, the underlying mechanism is still not clearly understood. More detailed studies are required in the future.

BIBLIOGRAPHY

1. Lohse, D., *Bubble puzzles*. Phys. Today, 2003. **56**: p. 36.
2. Ajaev, V.S. and G. M. Homsy, *Modeling shapes and dynamics of confined bubbles*. Annu. Rev. Fluid Mech., 2006. **38**: p. 277–307.
3. Gravesen, P., J. Branebjerg, and O. S. Jensen, *Microfluidics—a review*. J. Micromech. Microeng., 1993. **3**: p. 168–182.
4. Jensen, M.J., G. Goranovic, and H. Bruus, *The clogging pressure of bubbles in hydrophilic microchannel contractions*, . J. Micromech. Microeng., 2004. **14**: p. 876–883.
5. Elwenspoek, M., et al., *Towards integrated microliquid handling systems*. J. Micromech. Microeng., 1994: p. 227–245.
6. Nielsen, N.J., *History of thinkjet printhead development*, . Hewlett–Packard J., 1985. **36**: p. 4-10.
7. L. W. Lin, *Microscale thermal bubble formation: Thermophysical phenomena and applications*,. Microscale Thermophys. Eng., 1998. **2**: p. 71–85.
8. Jr-Hung Tsai and L. Lin, *A thermal-bubble-actuated micronozzle-diffuser pump*. Journal of Microelectromechanical Systems, 2002. **11**(6): p. 665-671.
9. Olsson A, S. G, and S. E, *A valve-less planar fluid pump with 2 pump chambers* Sensors Actuators A 1995. **47**: p. 549–556.
10. Yuan, H. and A. Prosperetti, *The pumping effect of growing and collapsing bubbles in a tube* J. Micromech. Microeng, 1999. **9**: p. 402–413.
11. TK, J. and K. CJ, *Valveless pumping using traversing vapor bubbles in microchannels*. . J Appl Phys 1998. **83**: p. 5658-5664.

12. Taylor, R.S. and C. Hnatovsky, *Trapping and mixing of particles in water using a microbubble attached to an nsom fiber probe*. Opt. Express, 2004. **12**: p. 916–928.
13. R. B. Maxwell, et al., *A microbubble-powered bioparticle actuator*. J. Microelectromech. Syst., 2003. **12**: p. 630–640.
14. S. Z. Hua, et al., *Microfluidic actuation using electrochemically generated bubbles*. Anal. Chem., 2002. **74**: p. 6392–6396.
15. D. A. Ateya, A.A. Shah, and S. Z. Hua, *Impedance-based response of an electrolytic gas bubble to pressure in microfluidic channels*. Sens. Actuators, A., 2005. **122**: p. 235–241.
16. D. A. Ateya, A.A. Shah, and S. Z. Hua, *An electrolytically actuated micropump*. Rev. Sci. Instrum., 2004. **75**: p. 915–920.
17. Hua, S.Z., et al., *Microfluidic actuation using electrochemically generated bubbles*. Anal. Chem., 2002. **74**: p. 6392–6396.
18. Leighton, T.G., *The acoustic bubble*. 1994: Academic Press, London.
19. Elder, S.A., *Cavitation Microstreaming*. J. Acoust. Soc. Am., 1959(31): p. 54-64.
20. Paul Tho, R. Manasseh, and A. Ooi, *Cavitation microstreaming patterns in single and multiple bubble systems*. J. Fluid Mech., 2007(576): p. 191-233.
21. Ketterling, J.A. and J. Mamou, *Excitation of polymer-shelled contrast agents with high-frequency ultrasound*. J. Acoust. Soc. Am., 2006. **121**(1): p. EL48-EL53.
22. Dayton, P.A., et al., *A preliminary evaluation of the effects of primary and secondary radiation forces on acoustic contrast agents*. Ultrasonics, Ferroelectrics and Frequency Control, IEEE Transactions on, 1997. **44**(6): p. 1264-1277.
23. Miller, D.L. and J. Quddus, *Sonoporation of monolayer cells by diagnostic ultrasound activation of contrast-agent gas bodies*. Ultrasound in Medicine & Biology, 2000. **26**(4): p. 661-667.
24. R. Bekeredjian, P. A. Grayburn, and R. V. Shohet, *Use of ultrasound contrast agents for gene or drug delivery in cardiovascular medicine*. Journal of the American College of Cardiology, 2005. **45**(3): p. 329-335.
25. P. Marmottant, S.H., *Controlled vesicle deformation and lysis by single oscillating bubbles*. Nature, 2003(12): p. 153-156.

26. Marmottant, P. and S. Hilgenfeldt. *A bubble-driven microfluidic transport element for bioengineering*. in *Proc. Natl. Acad. Sci.* 2004. U.S.A.
27. Chung, S.K., et al. *Micro Bubble Fluidics by EWOD and Ultrasonic Excitation for Micro Bubble Tweezers*. in *20th International Conference on Micro Electro Mechanical Systems (MEMS 2007)*. 2007.
28. Zhao, Y. and S.K. Cho, *Micro Bubble Manipulation by Electrowetting on Dielectric: transporting, splitting, merging and eliminating of bubbles*. *Journal of Lab a Chip*, 2007. **7**(2): p. 273-280.
29. Kuznetsova, L.A., et al., *Cavitation bubble-driven cell and particle behavior in an ultrasound standing wave*. *J. Acoust. Soc. Am.*, 2005. **117**(1): p. 104-112.
30. Laser, D.J. and J.G. Santiago, *A review of micropumps*. *Journal of Micromechanics and Microengineering*, 2004(6): p. R35.
31. Tsai, N.-C. and C.-Y. Sue, *Review of MEMS-based drug delivery and dosing systems*. *Sensors and Actuators A*, 2007. **134**: p. 555-564.
32. Robin H. Liu, a.J.Y., a Maciej Z. Pindera, Mahesh Athavale and Piotr Grodzinski, *Bubble-induced acoustic micromixing*. *Lab Chip*, 2002(2): p. 151-157.
33. Wu, N.-T.N.a.Z., *Micromixers—a review*. *J. Micromech. Microeng.*, 2005. **15**: p. R1-R16.
34. Garstecki, P., et al., *Mixing with bubbles: a practical technology for use with portable microfluidic devices*. *Lab Chip*, 2006. **6**: p. 207-212.
35. Oh, K.W. and C.H. Ahn, *A review of microvalves*. *J. Micromech. Microeng.*, 2006. **16**: p. R13-39.
36. Cho, S.K. and C.-J.C. Kim. *Particle Separation and Concentration Control for Digital Microfluidics*. in *The 16th Annual IEEE International Conference on MEMS (MEMS 2003)*. 2003. Kyoto, Japan.
37. Y. Zhao, U.-C. Yi, and S. K. Cho, *Micro Particle Concentration and Separation by Travelling Wave Dielectrophoresis (twDEP) for Digital Microfluidics*. *Journal of Microelectromechanical Systems*, 2007. **16**(6): p. 1472-1481.
38. Cho, Y.Z.a.S.K., *Microparticle Sampling by Electrowetting-Actuated Droplet Sweeping*. *Lab Chip*, 2006. **6**: p. 137-144.

39. Zhao, Y., et al. *Micro Particle Sampling on Microfabricated Perforated Filter Membranes*. in *The 11th International Conference on Miniaturized Systems for Chemistry and Life Sciences (μ TAS 2007)*. 2007. Paris, France.
40. Smits, J.G., *Piezoelectric micropump with 3 valves working peristaltically*. *Sensors Actuators A* 1990. **21**: p. 203–6.
41. Richter M, L. R, and W. P, *Robust design of gas and liquid micropumps* *Sensors Actuators A* 1998. **68**: p. 480–486.
42. Zengerle R, U.J., Kluge S, Richter M and Richter A, *A bidirectional silicon micropump* *Sensors Actuators A*, 1995. **50**: p. 81–86.
43. van de Pol F C M, et al., *A thermopneumatic micropump based on micro-engineering techniques* *Sensors Actuators A*, 1990 **21**: p. 198–202.
44. C, J.O. and Y.S. S, *Fabrication and test of a thermopneumatic micropump with a corrugated p+ diaphragm* *Sensors Actuators A* 2000. **83**: p. 249–55.
45. Benard W L, K.H., Heuer A H and Huff M A, *Thin-film shape-memory alloy actuated micropumps*. *J. Microelectromech. Syst.*, 1998. **7**: p. 245–51.
46. Bohm S, O.W.a.B.P., *A plastic micropump constructed with conventional techniques and materials*. *Sensors Actuators A* 1999. **77** p. 223–228.
47. Yun K-S, C.I.-J., Bu J-U, Kim C-J and Yoon E *A surface-tension driven micropump for low-voltage and low-power operations* *J. Microelectromech. Syst.*, 2002. **11**: p. 454–61.
48. E, K.D. and T.S. M, *Patterning liquid flow on the microscopic scale* *Nature* 1999. **402**: p. 794–7.
49. S, S.T. and B.M. A, *Thermocapillary pumping of discrete drops in microfabricated analysis devices* *AIChE J.* , 1999. **45**: p. 350–66.
50. Richter A, et al., *A micromachined electrohydrodynamic (EHD) pump*. *Sensors Actuators A* 1991. **29**: p. 159–168.
51. Darabi J, O.M. M, and D. D, *An electrohydrodynamic polarization micropump for electronic cooling* *J. Microelectromech. Syst.* , 2001 **10**: p. 98–106.
52. Jacobson S C, et al., *Open-channel electrochromatography on a microchip*. *Anal. Chem.*, 1994. **66**: p. 2369-73.

53. Laser, D.J., et al. *SILICON ELECTROOSMOTIC MICROPUMPS FOR INTEGRATED CIRCUIT THERMAL MANAGEMENT*. in *Proc. Transducers'03 (Boston, MA)*. 2003.
54. S, J.J. and L.S. S, *Theoretical and experimental study of MHD (magnetohydrodynamic) micropump*. *Sensors Actuators A* 2000. **80**: p. 84–9.
55. V, L.A. and L.A. P, *An AC magnetohydrodynamic micropump* *Sensors Actuators B* 2000. **63**: p. 178–185.
56. R J Dijkink, J.P.v.d.D., C D Ohl and A Prosperetti, *The ‘acoustic scallop’: a bubble-powered actuator*. *J. Micromech. Microeng.*, 2006(16): p. 1653-1659.
57. Minnaert, M., *On musical air-bubbles and the sound of running water*. *Philosophical Magazine*, 1933. **16**: p. 235–248.
58. Xu, J. and D. Attinger, *Acoustic excitation of superharmonic capillary waves on a meniscus in a planar microgeometry*. *PHYSICS OF FLUIDS*, 2007. **19**: p. 108107.
59. Marmottant, P. and S. Hilgenfeldt, *A bubble-driven microfluidic transport element for bioengineering*. *Proceedings of the National Academy of Sciences*, 2004. **101**(26): p. 9523-9527.
60. Ho, C.T., et al., *Micromachined electrochemical T-switches for cell sorting applications*. *Lab on a Chip*, 2005. **5**(11): p. 1248-1258.
61. K. Yanagiada, et al., *The usefulness of a piezomicromanipulator in intracytoplasmic sperm injection in humans*. *Human Reproduction*, 1998. **14**(2): p. 448-453.
62. T. Nakayama, et al., *A new assisted hatching technique using a piezo-micromanipulator*. *Fertility and Sterility*, 1998. **69**: p. 784-788.
63. Ashkin, A., *Applications of Laser Radiation Pressure* *Science*, 1980. **210**(4474): p. 1081-1088.
64. Svoboda K and B. SM, *Biological applications of optical forces*. *Annu Rev Biophys Biomol Struct.*, 1994. **23**: p. 247-85.
65. Voldman J, et al., *A microfabrication-based dynamic array cytometer*. *Anal Chem*, 2002. **74**(16): p. 3984-3990.
66. Schnelle T, et al., *Three-dimensional electric field traps for manipulation of cells-- calculation and experimental verification*. *Biochim Biophys Acta*, 1993. **1157**(2): p. 127-40.

67. Y., Y. and N. Y., *Micro particle trapping by opposite phases ultrasonic travelling waves* Ultrasonics,, 1998. **36**(8): p. 873-878.
68. Yamanouchi, M.T.a.K., *Ultrasonic Micromanipulation of Small Particles in Liquid* Jpn. J. Appl. Phys, 1994. **33**: p. 3045-3047.
69. Cho, C.-C., R.M. Wallace, and L.A. Files-Sesler, *Patterning and etching of amorphous teflon films* Journal of Electronic Materials, 1994. **23**(8): p. 827-830.
70. D, C.-Y., M. D, and G.B. K. *A novel PDMS microfluidic spotter for fabrication of protein chips and microarrays* in *Proc. SPIE* 2005.
71. Xia, Y. and G.M. Whitesides, *SOFT LITHOGRAPHY*. Annu. Rev. Mater. Sci., 1998. **28**: p. 153-184.
72. Lippmann, M.G., *Relations entre les phénomènes électriques et capillaires*. Ann. Chim. Phys., 1875. **5**: p. 494-549.
73. J. Lee, H.M., et al., *Addressable micro liquid handling by electric control of surface tension*. Proc. IEEE Int. Conf. MEMS, 2001.
74. J. Lee, et al., *Electrowetting and electrowetting-on-dielectric for microscale liquid handling*. Sens. Actuators, Phys. A, 2002. **95**: p. 259-268.
75. S. K. Chung, Y.Z., and S. K. Cho, *On-chip creation and elimination of microbubbles integrated with EWOD actuations toward micro-object manipulator*. Journal of Micromechanics and Microengineering 2008: p. in press.
76. Barry R. Lutz, Jian Chen, and D.T. Schwartz, *Hydrodynamic Tweezers: I. Noncontact Trapping of Single Cells Using Steady Streaming Microeddies*. Anal. Chem., 2006. **78**: p. 5429-5434.
77. Hu, J., et al., *Trapping, transportation and separation of small particles by an acoustic needle* Sensors and Actuators A: Physical, 2007. **138**(1): p. 187-193.
78. Kao, J., et al., *A bubble-powered micro-rotor: conception, manufacturing, assembly, and characterization*. Journal of Micromechanics and Microengineering, 2007. **17**: p. 2454-2460.